IMPROVEMENTS TO THE TRANSFER FUNCTION METHOD FOR DETERMINING THE COMPLEX DYNAMIC MODULUS OF POLYMER COMPOSITES

A. E. Semple
W. Thompson, Jr.

Technical Memorandum
File No. TM No. 85-138
5 August 1985
Contract No. N00014-84-0343

Copy No. 10

The Pennsylvania State University
Intercollege Research Programs and Facilities
APPLIED RESEARCH LABORATORY
Post Office Box 30
State College, Pennsylvaina 16804

NAVY DEPARTMENT

NAVAL SEA SYSTEMS COMMAND

UNCLASSIFIED

SECURITY CLASSIFICATION OF THIS PAGE (When Data Entered)

REPORT DOCUMENTATION PAGE		READ INSTRUCTIONS BEFORE COMPLETING FORM
1. REPORT NUMBER 85-138	2. GOVT ACCESSION NO.	3. RECIPIENT'S CATALOG NUMBER
4. TITLE (and Subtitle) Improvements to the Transfer Function Method for Determining the Complex Dynamic Modulus of Polymer Composites		5. TYPE OF REPORT & PERIOD COVERED Interim 6. PERFORMING ORG. REPORT NUMBER
7. AUTHOR(s) A. E. Semple W. Thompson, Jr.		8. CONTRACT OR GRANT NUMBER(s) N00014-84-0343
9. PERFORMING ORGANIZATION NAME AND ADDRESS APPLIED RESEARCH LABORATORY The pennsylvania State University Post Office Box 30, State College, PA 16804		10. PROGRAM ELEMENT, PROJECT, TASK AREA & WORK UNIT NUMBERS
11. CONTROLLING OFFICE NAME AND ADDRESS Office of Naval Research/Robert Pohanka 800 North Quincy St. Arlington, VA 22217		12. REPORT DATE 8/5/85 13. NUMBER OF PAGES 95
14. MONITORING AGENCY NAME & ADDRESS(if different from Controlling Office)		15. SECURITY CLASS. (of this report) UNCLASSIFIED 15a. DECLASSIFICATION DOWNGRADING SCHEDULE

16. DISTRIBUTION STATEMENT (of this Report)

APPROVED FOR PUBLIC RELEASE; DISTRIBUTION UNLIMITED

17. DISTRIBUTION STATEMENT (of the abstract entered in Block 20, if different from Report)

18. SUPPLEMENTARY NOTES

19. KEY WORDS (Continue on reverse side if necessary and identify by block number)

20. ABSTRACT (Continue on reverse side if necessary and identify by block number)

The Materials Research Laboratory at The Pennsylvania State University fabricates diphasic transducer composites made from polymers and piezoceramic. It is desired to measure the loss factor of these materials over the audible frequency range. After consideration of a number of measuring systems, a decision was made to implement the Transfer Function Method. This method consists of exciting a mass-loaded rod into longitudinal vibrations. The

DD FORM 1 JAN 73 1473 EDITION OF 1 NOV 65 IS OBSOLETE

UNCLASSIFIED

SECURITY CLASSIFICATION OF THIS PAGE (When Data Entered)

complex acceleration ratio between its ends is related to the dynamic modulus by two, coupled, transcendental equations derived by applying appropriate boundary conditions to the solution of the longitudinal wave equation. In theory, these equations can be solved at any frequency by an iterative procedure. In practice, convergence problems reduce the valid solutions to just those obtained at the longitudinal resonance frequencies. Improvements made during this study, enable the equations to be solved at any frequency except those were the phase of that ratio is zero. Plots of loss factor and storage modulus are presented for a number of composites. Several high-damping polymeric materials were also tested. A comparison between the present results and those quoted in other studies indicates that the improved method produces reliable results more quickly and with much less effort than previously required.

APPLIED RESEARCH LABORATORY
The Pennsylvania State University
Post Office Box 30
State College, Pennsylvania 16804

From: A. E. Semple and W. Thompson, Jr.

Subject: Improvements to the Transfer Function Method for Determining the Complex Dynamic Modulus of Polymer Composites

Abstract:

The Materials Research Laboratory at The Pennsylvania State University fabricates diphasic transducer composites made from polymers and piezoceramic. It is desired to measure the loss factor of these materials over the audible frequency range. After consideration of a number of measuring systems, a decision was made to implement the Transfer Function Method. This method consists of exciting a mass-loaded rod into longitudinal vibrations. The complex acceleration ratio between its ends is related to the dynamic modulus by two, coupled, transcendental equations derived by applying appropriate boundary conditions to the solution of the longitudinal wave equation. In theory, these equations can be solved at any frequency by an iterative procedure. In practice, convergence problems reduce the valid solutions to just those obtained at the longitudinal resonance frequencies. Improvements made during this study, enable the equations to be solved at any frequency except those were the phase of that ratio is zero. Plots of loss factor and storage modulus are presented for a number of composites. Several high-damping polymeric materials were also tested. A comparison between the present results and those quoted in other studies indicates that the improved method produces reliable results more quickly and with much less effort than previously required.

TABLE OF CONTENTS

LIST OF FIGURES

Figure | Page

LIST OF TABLES

LIST OF SYMBOLS

a = radius of a cylindrical sample

a_T = WLF shift factor

A = cross-sectional area of bar

A_r = resonance amplification factor

c = complex phase velocity

c_1 = viscoelastic shift constant

c_2 = viscoelastic shift constant

c' = viscous damping coefficient

c_c = critical viscous damping coefficient

E' = storage modulus of elasticity

E'' = loss modulus of elasticity

E_a = apparent storage modulus of elasticity

E^* = complex modulus of elasticity

E_r^* = resultant complex modulus of elasticity

f = frequency, Hz

f_n = natural frequency, Hz

Δf = frequency bandwidth between half power points, Hz

F = force at any section of the bar

G^* = complex shear modulus

h = thickness of beam in the plane of bending

LIST OF SYMBOLS (Cont)

i = $(-1)^{1/2}$

I = second moment area of the cross section

J_n = Bessel function of the first kind of order n

k = complex wave number (ω/c)

k_n = constant which depends upon the mode number and damping method

K_m = correction factor for antiresonances

K_n = correction factor for resonances

L = length of the bar

m = mass of the bar

M = end mass

n = mode number

Q = mechanical quality factor

r_g = radius of gyration about the x axis

R = mass ratio, (M/m)

S = shape factor

t = time, seconds

T_0 = reference temperature, °C

T_{60} = time for signal to decrease by 60 dB, seconds

T_R = real part of the ratio of acceleration of the driven end of the bar to that of the mass loaded end

LIST OF SYMBOLS (Cont)

T_I = imaginary part of the ratio of acceleration of the driven end of the bar to that of the mass loaded end

u = axial displacement at any section of the bar

x = axial coordinate of the bar

X_n = dimensionless constant dependent upon boundary conditions

β = constant based on the volume-stress function

δ = angle by which strain lags stress

Δ = logarithmic decrement

ζ = damping ratio, (c'/ c_c)

η = elastic loss factor

η_a = apparent elastic loss factor

η_G = shear loss factor

η_ν = Poisson loss factor

λ_f = wavelength

ν' = storage Poisson ratio

ν'' = loss Poisson ratio

ν^* = complex Poisson ratio

ξ = frequency ratio $(\omega L/c)$

ρ = density of bar

σ_L = stress sensitivity limit

LIST OF SYMBOLS (Cont)

ϕ = phase angle between force and displacement

ψ = specific damping capacity

ω = radian frequency, rad/s

ω_n = natural radian frequency, rad/s

Ω = damping parameter, $\tan(\delta/2)$

CHAPTER 1

INTRODUCTION

1.1 Problem Definition

Recent improvements in the development of diphasic polymer composites have lead to the formulation of materials with improved mechanical and/or electrical properties as compared with single phase materials. The Nippon Electric Co., Ltd (NEC) has succeeded in developing a ferrite compound which is structurally stiff (compressive strength: 150 x 10^6 N/m^2), yet possesses desirably high damping (100 times that of iron or aluminum) [1]. The material consists of ferrite particles embedded in a polyester resin. It is postulated that the high specific gravity particles resonate with the elastic resin causing high internal damping.

In a similar vein, the Materials Research Laboratory (MRL) at The Pennsylvania State University, has been fabricating diphasic transducer materials made from polymers and piezoelectric ceramics. When composite transducers are driven at high frequencies they sometimes exhibit a mode of vibration in which the component materials vibrate out of phase. Internal friction between the filler and matrix materials causes the damping. Additional damping, due to electromechanical energy conversion and ohmic dissipation may also be realized if the piezoceramic particles are polarized.

A method of measuring damping properties in the frequency range 0 to

20 kHz, for a composite of limited size, was necessary for acoustic loss comparison. Since damping properties are a strong function of frequency for viscoelastic materials, the method also had to be capable of computing the damping values as a function of frequency.

After consideration of various procedures to measure the dynamic modulus of elasticity, a technique using the acceleration transfer ratio between the two ends of a mass loaded rod was selected [2-5]. A long thin sample is excited into longitudinal vibration and the relative amplitude and phase information recorded at frequencies in the audible range. The amplitude ratio and phase at the longitudinal resonances (phase= ±90°) is related to the elastic modulus and loss factor (η) by a pair of coupled, nonlinear, transcendental equations derived from solving the equation of motion of a mass-loaded rod excited into longitudinal vibrations. In theory, the equations can be solved at any frequency, providing amplitude and phase information is known. In practice, convergence problems limit usable data to only the longitudinal resonances.

An improved computational algorithm has been developed which can yield loss and elastic modulus values at frequencies other than the ± 90° phase points. The method incorporates an improved "seed" formulation based on the behavior of the accelerometer transfer function. This algorithm facilitates the solution of the equations while reducing the computation time.

1.2 Discussion of Damping

The dynamic characteristics of a structure can be determined through the characterization of the mass, stiffness, and damping. The mass can be easily ascertained using static measurements. The dynamic stiffness is a complex mechanism which almost always requires a dynamic test setup. Damping relates the energy dissipated to the energy stored in the material.

Each dynamic characteristic possesses an energy analogy. Kinetic energy is associated with the mass, potential energy is related to the stiffness, and damping is a measure of system energy losses. Damping energy is usually dissipated as heat.

The mechanisms of damping are many. Interface friction, internal friction, fluid viscosity, turbulence, acoustic radiation, eddy currents, and magnetic hysteresis are some of the major ones [6]. Internal and interface friction constitute the most common types of damping. Friction mechanisms include: plastic slip, plastic flow, dislocation movements, and inhomogeneous strain in fibrous materials [7]. Due to the polymeric nature of the materials tested in this study, molecular curling and uncurling of polymers may also be a major source of damping.

The majority of the materials tested in this study can be classified as viscoelastic. Viscoelastic composites display both time and temperature dependent properties. All linear viscoelastic materials possess a complex modulus of elasticity:

$$E^* = E' + iE'' = E'(1 + i\eta) = E' e^{i\delta} \qquad (1.1)$$

where,

E^* = complex modulus of elasticity

E' = storage modulus of elasticity

E'' = loss modulus of elasticity

η = loss factor

δ = phase lag between stress and strain

Typical plots of both the storage modulus and loss factor versus frequency or temperature for a viscoelastic material are shown in Fig. 1.1 The loss factor (η) will be the only measurement unit for damping used in this study. No standard nomenclature for damping exists at this time. This is due in part to the great variety of applications of damping for both engineering purposes as well as purely academic uses. For specimens with uniform lateral stress distributions the following damping relationships exist [7]:

$$\eta = \tan\delta = \Delta/\pi = \psi/2\pi = 2\zeta/(1-\zeta^2)^{1/2} = \Delta f/f_n = 1/A_r = 1/Q \qquad (1.2)$$

where,

Δ = logarithmic decrement.

ψ = specific damping capacity.

ζ = the damping ratio (c'/c_c).

$\Delta f/f_n$ = bandwidth at the half power points/natural frequency.

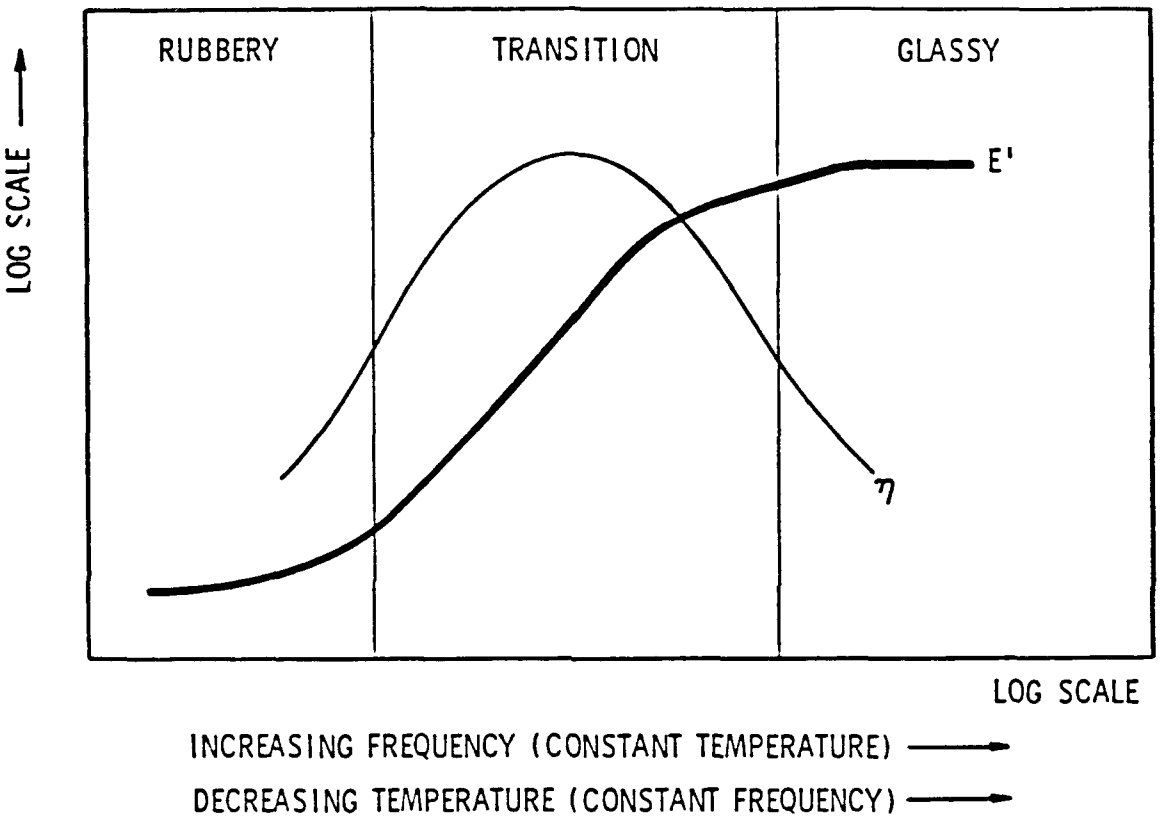

Figure 1.1 Dependence of Modulus of Elasticity, E', and Loss Factor, η, on Temperature or Frequency

A_r = resonance amplification factor (induced force/exciting force).

Q = measure of sharpness of a resonance peak and amplification produced by resonance.

Along with the problems of not having a standard nomenclature, there are problems with documenting stress distributions and shape factors of the samples which are tested for damping. The loss factor is not truly independent of stress amplitude. As the stress amplitude increases the damping property of the material will also increase. If the stress is cyclical the number of fatigue cycles will have very little effect upon the damping up to a stress level known as the cyclic stress sensitivity limit σ_L. Above this value, stress at approximately 80 per cent of the fatigue limit, the damping will again increase [8].

Likewise, the relative dimensions of a specimen can affect the modulus of elasticity, E^*, and thus also affect the loss factor. For rubber-like materials the resultant modulus of elasticity is given by [9]:

$$E_r^* = (1 + \beta S^2) E^* \qquad (1.3)$$

where E_r^* = resultant complex modulus of elasticity.

β = numerical constant based on volume-stress function and the stress distribution. (β usually equals 2.0)

S = shape factor (loaded surface area/remaining surface area)

1.3 Complex Modulus Measurement Techniques

An abundance of techniques exists for measuring the damping properties of materials. Two of the classic methods are the Frequency Response Method and the Reverberation Method [10]. The Frequency Response Method entails vibrating a cantilevered specimen at its resonance frequencies and recording the vibration amplitudes, preferably on a dB scale. By taking the frequency bandwidth between the two -3 dB points relative to the peak, the loss factor and storage modulus can be calculated from:

$$\eta = \Delta f_n / f_n \tag{1.4a}$$

$$E' = 38.24\, \rho L^4 f_n^2 / h^2 \tag{1.4b}$$

where, ρ = sample density (kg/m^3).

L = unsupported length (cm).

h = thickness in the direction of vibration (cm).

The Reverberation Method uses a measure of the vibration decay rate of a specimen. To perform the test, the sample must be excited into vibrations at any resonance frequency until steady state conditions are achieved. When the exciting force is suddenly removed, the resulting decay curve can be used to ascertain the loss factor:

$$\eta = 2.2 / T_{60} f_n \tag{1.5}$$

where, T_{60} = the time in seconds for the vibration level to decrease 60 dB.

Nearly all methods for determining the complex modulus of elasticity can be grouped into one of the following seven measurement categories [11];

the shape, size and homogeneity of the sample will greatly determine which method should be used:

1. Transverse Resonance Mode Vibration - A small bar-like sample is excited into transverse vibration at one end using a non-contact transducer while a second non-contact transducer picks up the displacement of the other end. A plot of displacement versus frequency is used to determine the loss factor (-3 dB bandwidth method) and the storage modulus is found using Eq. (1.6).

$$E' = 4.8\pi^2\rho[L^2 f_n/hk_n^2] \tag{1.6}$$

The coefficient k_n depends upon the mode number and damping method.

2. Forced Vibration - Used primarily for large, highly damped specimens. The specimen is fixed at the two ends and driven transversely, at a constant displacement, at its middle using a sinusoidal force F. The equations for computing the loss factor and storage modulus are:

$$E' = [F\cos\phi/y + 2\pi^2 f^2 LA\rho]2L^3/I\pi^4 \tag{1.7}$$

$$\eta = [1 - y4\pi^2 f^2 LA\rho/F2\cos\phi]\tan\phi \tag{1.8}$$

The parameter y is the displacement of the bar's middle, I is the second moment of area of the cross section of area A, and ø is the phase angle between force and displacement.

3. Flexural Wave Method - A probe microphone is used to scan the length of a transversely vibrating beam, mounted on flexible supports, to determine the resonances from the node locations. Using the input

frequency and material parameters the storage modulus can be computed from Eq. (1.9):

$$E' = f_n^2 4\pi^2 \rho A L^4 / X_n^4 I \qquad (1.9)$$

The constant X_n is dimensionless and dependent upon the boundary conditions.

4. Mechanical Impedance Method - A small specimen is driven longitudinally at a constant velocity using an impedance head. A force vs. frequency plot is made and the loss factor is determined from the -3 dB bandwidth. The storage modulus at the resonances (n) and antiresonances (m) is found from Eqs. (1.10) and (1.11).

$$E' = \rho[2Lf_n/n]^2/K_n \qquad (1.10)$$

$$E' = \rho[2Lf_m/m-1/2]^2/K_m \qquad (1.11)$$

The constants K_n and K_m are correction factors.

5. Transfer Function Method - A bar sample, with accelerometers located at each end, is vibrated longitudinally. Using the amplitude and phase of the ratio of acceleration at the ends and the equations of motion for a mass-loaded rod the damping and storage modulus values can be computed. (also called the Phase Measurement Method)

6. Thin Fibers - Setup similar to the Transfer Function Method except the sample is loaded in tension. The loss factor is obtained from the -3 dB bandwidths at the resonance frequencies and the storage modulus is obtained using Eq. (1.12).

$$E' = 4\pi^2 f_n^2 L^2 \rho \qquad (1.12)$$

7. Vibration Decay Method - By suddenly removing the excitation force, after steady state conditions are achieved, the loss factor can be determined from Eq. (1.5) and the storage modulus from Eq. (1.12).

Several limitations on the size and compliance of the samples available for this study reduced the method choice to a couple of those listed above. First, the sample size had to be kept to a minimum for fabrication purposes. The maximum convenient size for mixing and hot pressing was approximately 8 cm by 1 cm^2. This eliminated the Forced Vibration (2) and Flexural Wave methods (3). Second, the samples would include a large number of very high damping materials so the resonance peaks would not always be apparent. This effectively ruled out the -3 dB measurement schemes, viz, the Transverse Resonance Mode Vibration (1), the Thin Fibers Method (6), and the Mechanical Impedance Method (4). And last, the samples were primarily too compliant for a technique requiring any amount of sample rigidity. The Flexural Wave Method (7) would not work well with extremely soft samples.

The method finally chosen was the Transfer Function or Phase Measurement Method. The procedure consists of exciting a bar-shaped specimen into longitudinal vibration and recording the complex ratio of the acceleration, or displacement, between the two ends. This decision was reaffirmed by the findings of a survey of current dynamic modulus

techniques that was undertaken in 1982 by Bolt Beranek and Newman Inc. [12].

That report ranks the available systems for testing the dynamic modulus of elastomers according to three cost ranges. A preliminary list of minimum requirements which all sytems had to meet was described. Some of the more important of these are:

1. The system measures at least one frequency between 200 and 8000 Hz.
2. The accuracy of the system is within ±20% in modulus or loss factor.
3. The technique must be capable of measuring two different materials.
4. The determination of modulus and loss factor takes less than 10 days.

A figure of merit was awarded to each system based upon a set of basic attributes. Typical attributes included: frequency and temperature range, accuracy, time per measurement, availability, range of sample size, and capability of computer interface. Table 1.1 assigns the attribute weights using three schemes. The attributes in the "average" column are assigned values according to rank of importance. The most important attribute, frequency and temperature range, received the most points (16.1 and 15.6) while the other attributes received decreasing values according to order of importance. The weightings in the column labeled "flat" are assigned by assuming that the attributes are nearly equal in importance with the more important attributes still receiving a few extra points. The "highly skewed" column gives a strong emphasis on frequency and temperature range. In all

Table 1.1 - Attribute Weightings from the BBN study [12].

Attribute	Average Weighting		Envelopes of Weightings Proposed			
	Compressive Load	Tensile Load	Compressive Load		Tensile Load	
			"Flat"	"Highly Skewed"	"Flat"	"Highly" Skewed"
Frequency & Temperature Range	16.1	15.6	10.6	40.0	10.6	38.9
Static Modulus Range	12.1	11.7	10.1	10.0	10.1	9.8
Accuracy	11.0	10.6	9.6	10.0	9.6	9.8
Meas. Time/Measurement	10.5	10.2	9.0	10.0	9.0	9.8
Availability/Risk	9.0	8.8	8.0	10.0	7.9	9.8
Equipment Reliability	8.2	8.0	8.0	4.0	7.9	3.9
Total Meas. Time/Sample	7.7	7.5	7.45	4.0	7.4	3.9
Frequency Sampling	6.8	6.6	7.45	4.0	7.4	3.9
Effective Properties	5.2	5.0	7.45	4.0	7.4	3.9
Static Load & Pressure Range	5.0	8.0	7.45	2.0	7.9	3.9
Computer Interface	4.2	4.0	7.45	1.0	7.4	1.2
Sample Type	4.2	4.0	7.45	1.0	7.4	1.2

cases the total point value of all the attributes had to add up to 100.

Table 1.2 gives a summary of the Figures of Merit for the evaluated systems. The systems are grouped into three cost ranges. "Type" refers to the seven measurement categories enumerated previously. Several of the methods shown involve using the Transfer Function Method. Notice that the top performer in the least expensive group, the NSWC Transfer Function Test, received nearly as many points as the top two performers in the most expensive group.

Based on this study and the limitations previously mentioned, a decision was made to implement the Transfer Function Method for the present study. The BBN study gives the following information for the NSWC Transfer Method:

Frequency: 200 to 25,000 Hz.

Accuracy : ±5%

Temperature: 0 to 50°C.

Static Modulus: 10^5 to 10^{11} dynes/cm^2.

The Transfer Function Method looked particularly attractive since all of the necessary electronic measuring equipment already existed and could be linked to an HP 9825B computer. The only piece of equipment which needed to be fabricated was a test stand to hold the shaker and sample. Chapter Two details some of the particulars of the Transfer Function Method and also describes the improvements made to the method during this study.

Table 1.2 - Figures of Merit and Relative Costs for Qualifying Systems from the BBN study [12].

System	Type	Compressive Load			Tensile Load		
		Average	Flat	Highly Skewed	Average	Flat	Highly Skewed
Most Expensive							
Metravib MAK 03	2	90.8	92.4	84.1	91.1	92.4	85.5
MTS Dynamic Test System	4	90.8	92.4	84.1	91.1	92.4	85.5
Dynastat/Dynalyzer	1	89.9	92.7	79.0	90.2	92.7	79.6
NRL-String/Thin Rod	5	87.5	84.1	91.7	89.4	86.4	92.4
Medium Expense							
Instron 1350/Dynalyzer	1	92.0	94.7	80.0	92.2	94.7	80.6
NSWC String Apparatus	6	82.0	77.9	87.7	84.1	81.0	88.5
BBN Transfer Function Test	5	78.4	78.9	83.0	77.2	77.4	82.2
Vibrating Beam (w/comp)	1	77.9	82.3	83.1	78.0	74.9	83.0
DTNSRDC String Apparatus	6	74.8	71.6	82.6	76.7	73.9	72.8
Optical Measurement	3	74.4	70.7	71.7	76.7	73.1	72.8
Comparison Techn. (w/comp)	3	74.2	74.3	71.9	73.6	71.9	72.1
Transfer Function Method	5	73.4	72.6	78.3	71.9	70.4	77.4
Least Expensive							
NSWC Transfer Funct. Test	5	89.6	86.4	92.7	89.4	86.4	92.4
B & K Complex Mod. App.	1	78.4	73.2	83.3	80.2	74.8	83.8
Vibrating Beam	1	73.7	74.8	82.1	74.0	67.5	81.8
Dynamic Mech. Spectrometer	5	73.5	70.2	70.7	73.8	70.3	73.2
E. B. String Test	3	70.5	69.4	77.2	72.9	71.7	78.1
Comparison Technique	1	69.2	64.4	70.9	69.6	64.5	70.9
Point Impedance	4	67.4	64.4	70.9	69.6	64.5	70.9
Transient Vibration Expt.	1	66.1	63.5	59.5	66.6	63.6	62.0
Tuned Damper	5	59.3	59.4	68.0	58.1	57.2	67.3

CHAPTER 2

THE TRANSFER FUNCTION METHOD

2.1 Theory and Overview

The technique of obtaining dynamic material parameters using the acceleration transfer ratio between the two ends of a bar-like specimen has been utilized since J. L. Quimby first used longitudinal beam vibrations to measure viscosity in 1925 [13]. At present, the transfer ratio and material parameters can be used along with the well known longitudinal wave propagation equation (Eq. (2.1)) to determine E' and E'' for a bar-like sample.

$$(E' + iE'')(\partial^2 u/\partial x^2) = \rho(\partial^2 u/\partial t^2) \qquad (2.1)$$

The loss factor, η, is simply E''/E'.

Not all of the longitudinal vibration techniques require the measurement of the acceleration transfer function. Galkiewicz and Karasz employed a longitudinal resonance technique but used the -3 dB amplitude method to obtain the logarithmic decrement [14]. Likewise, Ferguson uses a similar method for finding the loss using a triple-bar composite resonance technique [15]. D. I. G. Jones et. al. used a tuned damper technique to simplify both the equations of motion and the experimental procedure for determining the dynamic modulus of a short rod [16,17].

The present Transfer Function Method evolved as the result of two theoretical papers. Tung-Ming Lee combined the appropriate boundary

conditions and the longitudinal wave propagation equation to model a fixed-free bar [18]. Later, D. M. Norris, Jr. and Wun-Chung Young extended the solution to include a bar with an attached end mass [5]. The solution of a bar with an end mass is of practical importance since it is common to have a fixture, or at least an accelerometer, attached to the undriven end of the bar or rod. Norris and Young used both graphical and computer methods to solve the resulting two equations representing the real part, T_R, and imaginary part, T_I, of the acceleration ratio, or equivalently, the displacement ratio of the two ends. Equations (2.2) and (2.3) detail these two, coupled, transcendental equations. The complete derivation can be found in Appendix A.

$$T_R = \cosh[\xi\Omega](\cos\xi - R\xi\sin\xi) + R\xi\Omega\cos\xi\sinh[\xi\Omega] \tag{2.2}$$

$$T_I = \sinh[\xi\Omega](\sin\xi + R\xi\cos\xi) + R\xi\Omega\sin\xi\cosh[\xi\Omega] \tag{2.3}$$

where, R = mass ratio, $M/\rho AL$

M = the end mass

ξ = frequency parameter, $\omega L/c$

$\Omega = \tan(\delta/2)$

c = complex phase velocity, $(E^*/\rho)^{1/2}\sec(\delta/2)$

This experimental procedure has been successfully utilized by many people including Madigosky [2,19], Pritz [3], and Capps [4]. To obtain the storage modulus and the loss factor the solutions for ξ and δ should be inserted into Eqs. (2.4) and (2.5).

$$\eta = \tan(\delta) \tag{2.4}$$

$$E' = \rho(\omega L/\xi)^2 \cos^2(\delta/2) \cos(\delta) \qquad (2.5)$$

The method seems straightforward. Measure the transfer ratio between the end displacements or accelerations and solve the above equations using a computer to obtain the complex dynamic modulus. Unfortunately, several problems exist that limit both the accuracy and applicability of the Transfer Function Method.

2.2 Limitations of Present Transfer Function Method

While the Transfer Function Method seems to be gaining popularity as a dynamic modulus testing procedure, it still suffers some shortcomings in the form that most practitioners are using. These problems can be grouped into three categories: computer solution problems, data extension problems, and lateral vibration effects.

2.2.1 Computer Solution of the Coupled Equations

The computer solution of Eqs. (2.2) and (2.3) can be complicated. The most common approach is to use an iterative procedure such as the Newton-Raphson technique [20] to simultaneously solve the two coupled equations. This technique searches for the maxima or minima of the equations by locating the zeroes of the derivatives of the equations.

Although the Newton-Raiphson technique converges quickly to a root of the equations, there is no guarantee that it will be the correct root. It turns out that the number of possible roots for a given value of T_R , R, and T_I is

infinite; given any value of ξ, a value of Ω can be found which satisfies Eqs. (2.2) and (2.3). Like the solution to most eigenvalue problems, the roots are related to the mode number.

An often used approximation has been to chose a seed based upon neglecting the damping and solving the wave equation for the frequency parameter, ξ, at the resonance frequencies:

$$\xi = (2n-1)\pi/2(R+1) \qquad (2.6)$$

The mode number is given by "n". Using Eq. (2.6) to generate the iteration starting point, or "seed", the solution of Eqs. (2.2) and (2.3) at the resonance frequencies can be achieved with some degree of confidence. Correct solutions, or roots, are usually obtained for the first couple of modes. After this, the Newton-Raphson technique will often yield incorrect solutions. Thus, the judgment of a skilled operator will usually be necessary to discern the good roots from the bad. To further complicate matters, a certain amount of symmetry exists in Eqs. (2.2) and (2.3), that is, each positive root has a corresponding negative root which is close in magnitude. This false root can cause problems for investigators who are not careful about sign conventions. Depending upon the sample size and frequency range, a typical test will yield no more than five or six data points.

Low damping materials provide an additional problem for this measuring system. Whenever the phase angle of the acceleration ratio approaches 0°, the accuracy of the results becomes questionable. The solution of Eqs. (2.2) and (2.3) will result in loss factor values very close to

zero. The explanation for this can be understood by looking at Eq. 2.3. When the phase angle equals zero, T_1 will also equal zero. The imaginary portion of the acceleration transfer ratio equals zero at any frequency if the damping parameter is also equal to zero. Thus, Eqs. (2.2) and (2.3) will have two solutions, for the same value of ξ, $\tan(\delta/2)$, and R; one with a loss factor value near zero and one at the correct root. This is the primary reason why investigators have not attempted to solve the equations at nonresonance frequencies.

2.2.2 Three Methods for Extending Results

There are several ways to broaden the frequency range of the results. The simplest method involves varying the weight of the end mass. Increasing the end mass will shift the resonance frequencies to lower values. Conversely, a decrease in the end mass will raise the resonance frequencies with an absolute limit corresponding to the resonance frequencies of a free-free bar. Using this procedure, the resonances can be shifted to obtain results for a wide range of frequencies.

The second method for increasing the number of data points is to shift the resonances by varying the length of a sample. This will accomplish the same effect as the first method. A long sample will naturally have a lower primary resonance frequency than a short sample.

Using the present form of the Transfer Function Method, it is advantageous to shift the resonances up in frequency. The chance of

obtaining incorrect ξ and Ω values increases greatly for higher modes. By shifting the first few modes up in frequency, the range of believable results essentially shifts up in frequency. In addition, materials which are very compliant will not provide valid results at higher frequencies. This is due to the mass-loaded end accelerations being so small that the noise floor of the test equipment is approached. Some materials reach this noise limit at frequencies below 4 kHz.

The final means of extending the frequency range of useful data is applicable if the material is viscoelastic. A material which is viscoelastic will exhibit an increase in strain as a function of time and temperature when subjected to a constant stress. By recording damping and storage modulus data at various temperatures and using the time-temperature superposition principle [21], the frequency range of the data can be extended. The principle, as shown in Fig. 1.1, is based upon the theory that a decrease in temperature at a constant frequency causes the same change in dynamic material properties as an increase in frequency at a constant temperature. The frequency shift, corresponding to a change from some temperature T to a reference temperature T_0, is given by the WLF [21] equation:

$$\log a_T = -c_1 (T-T_0) / (c_2 + T-T_0) \qquad (2.7)$$

The shift factor a_T is equal to the shifted frequency divided by the reference frequency. The constants c_1 and c_2 are shift constants which are characteristic of each viscoelastic material at a given T_0. If the glass

transition temperature of the material T_g is used as the reference temperature, T_o, then c_1 and c_2 become the universal constants (c_1 = 17.44 and c_2 = 51.6). The WLF equation is primarily applicable for temperatures between T_g and T_g + 100°C. The use of the WLF shift equation can effectively extend the frequency range of the data several decades higher and lower from those over which valid data can be obtained at a single temperature.

Most of the Transfer Function Method results quoted in the literature have been enhanced using the WLF shift equation. The procedure can be time consuming and introduces additional errors due to inaccuracies in finding the shift constants and applying the shift factor a_T to the experimental data. In spite of this, the method stands as a useful tool for obtaining dynamic material properties at frequencies outside the range of test limits.

2.2.3 Lateral Motion Effect

The wave equation, Eq (2.1), is based on the assumption that wave propagation occurs only in the axial directions. This approximation is only valid if the lateral dimensions of the rod are small compared with the wavelength. A better equation, which takes into account the effect of lateral motions, is the Pochhammer-Chree frequency equation for longitudinal waves in an infinitely long cylinder [22]. Using the boundary condition that the cylindrical surface is traction-free and neglecting

torsional waves, the solution [23] to the frequency equation for longitudinal waves is:

$$(k^2-q^2)^2 [J_0(pa)/J_1(pa)] + 4k^2pq [J_0(qa)/J_1(qa)] - (2p/a)(k^2+q^2) = 0 \qquad (2.8)$$

where a = radius of the cylinder

$p = [(\omega^2\rho/E^*) - k^2]^{1/2}$

$q = [(\omega^2\rho/G^*) - k^2]^{1/2}$

k = complex wavenumber (ω/c)

Solving Eq. (2.8) for its roots yields the cutoff frequencies or eigenvalues. Pritz [24] and Snowdon [9] used a much less complicated approximation to the Pochhammer-Chree equation developed by Love [25]. The lateral motion is taken into account to some extent by the differential equation:

$$\rho [\partial^2u/\partial t^2 - (\nu^* r_g)^2 \partial^4u/\partial x^2\partial t^2] = E^* \partial^2u/\partial x^2 \qquad (2.9)$$

where $u(x)$ = axial displacement of the bar

ν^* = complex Poisson's ratio = $\nu'(1 + i\eta_\nu)$

r_g = radius of gyration about the x axis

For a sample with a square cross-section of area A, $r_g = (A/6)^{1/2}$.

Neglecting the lateral motion of the sample yields a storage modulus and a loss factor which deviate from the true values of E' and η when the lateral dimensions become an appreciable portion of the wavelength at higher frequencies. For a bar subjected to a time harmonic displacement, Eq. (2.9) becomes:

$$E'(1 + i\eta) = E'(1 + i\eta)[1 - [\rho/E'(1 + i\eta)]\omega^2 \nu'^2(1 + i\eta_\nu)^2 r_g^2] \quad (2.10)$$

The apparent storage modulus and apparent loss factor can be normalized by the true values of E' and η:

$$E_a'/E' = 1 - (\rho/E') \omega^2 (\nu' r_g)^2 (1 - \eta_\nu^2) \quad (2.11)$$

$$\eta_a/\eta = [1 - (\rho/E') \omega^2 (\nu' r_g)^2 2(\eta_\nu /\eta)] / (E_a'/E') \quad (2.12)$$

Assuming η_ν=0, Eqs. (2.11) and (2.12) can be placed in a form suitable for use as a correction factor for the apparent values (E_a' and η_a) obtained by using the elementary theory (Eq. 2.1).

$$E' = E_a' [1 + 4\pi^2 \nu'^2(r_g/\lambda_f)^2 (1 - \eta_\nu^2)] \quad (2.13)$$

$$\eta = \eta_a /[1 + 4\pi^2 \nu'^2(r_g/\lambda_f)^2 (1 - \eta_\nu^2 - 2\eta_\nu/\eta)] \quad (2.14)$$

where, λ_f = wavelength = $(1/f)(E_a'/\rho)^{1/2}$

The η on the right hand side of Eq. (2.14) can be approximated by η_a with little error. The assumption that η_ν is equal to zero can be justified by defining the real and imaginary portions of the Poisson's ratio in terms of the elastic and shear moduli and loss factors [9]:

$$\nu^* = (E^*/2G^*) - 1 \quad (2.15)$$

This can be separated into real and imaginary components:

$$\nu^* = \nu' + i\nu'' \quad (2.16)$$

where

$$\nu' = (E'/2G')[(1 + \eta\eta_G)/(1 + \eta_G^2)] - 1 \quad (2.17)$$

and

$$\nu'' = (E'/2G')[(\eta - \eta_G)/(1 + \eta_G^2)] \qquad (2.18)$$

For plastic and rubberlike materials the elastic loss factor, η, is very close to the shear loss factor, η_G, [9] making Eq. (2.18) approximately equal to zero. Since $\eta_\nu = \nu''/\nu'$, the Poisson loss factor will also be close to zero.

Without the corrections in Eqs. (2.13) and (2.14), the elementary theory will give storage modulus results at high frequencies which are too low while the loss factor values will be too high.

2.3 Improvements to the Transfer Function Method

A better understanding of the behavior of Eqs. (2.2) and (2.3) is instrumental in understanding why convergence problems occur when using the Newton-Raphson technique or any computer solution method. A visualization of the two equations as a function of the frequency parameter, ξ, and the damping parameter, $\tan(\delta/2)$, is obtained by making a three-dimensional grid plot. The plots in Figs. 2.1 and 2.2 give a compressed view of the real and imaginary components of the acceleration ratio. For $\xi = 20$, $R = 1.0$ and $\tan(\delta/2) = 2.0$ (corresponding to the highest points on the curves), T_R and T_I are of the order of 10^{17} and 10^{18} respectively; i.e. very large numbers. Consequently, these transfer function amplitudes are modified using a logarithmic scaling factor to compress both the positive and negative values so that the definition of the curve surfaces can readily be discerned. This scaling is performed as follows: the logarithm of the positive values greater than 1 are plotted, the logarithm of the absolute

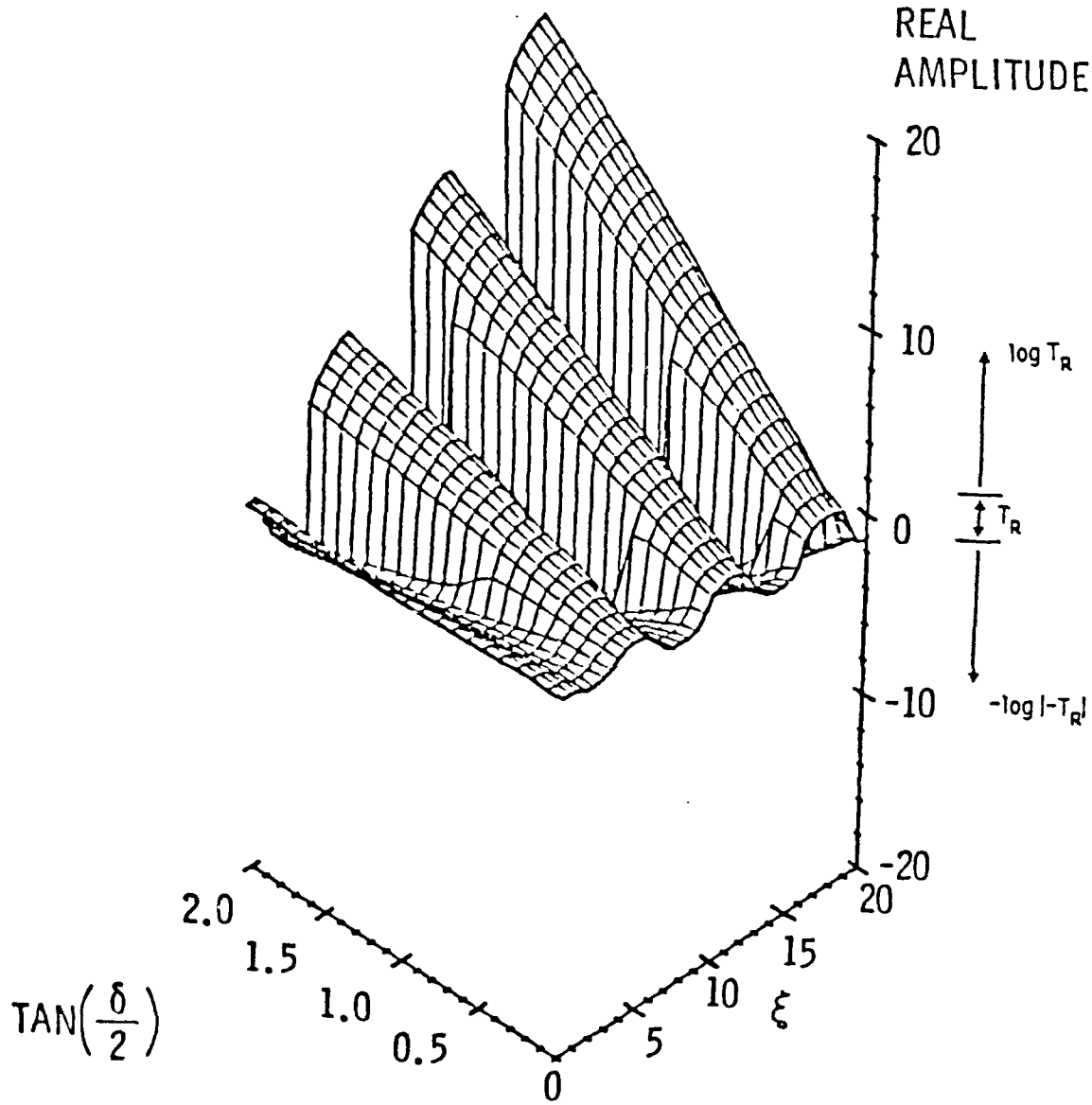

Figure 2.1 Three-Dimensional Grid Plot of the Real Transfer Function Amplitude as a Function of ξ and tan(δ/2) for an Assumed Mass Ratio R= 1.0.

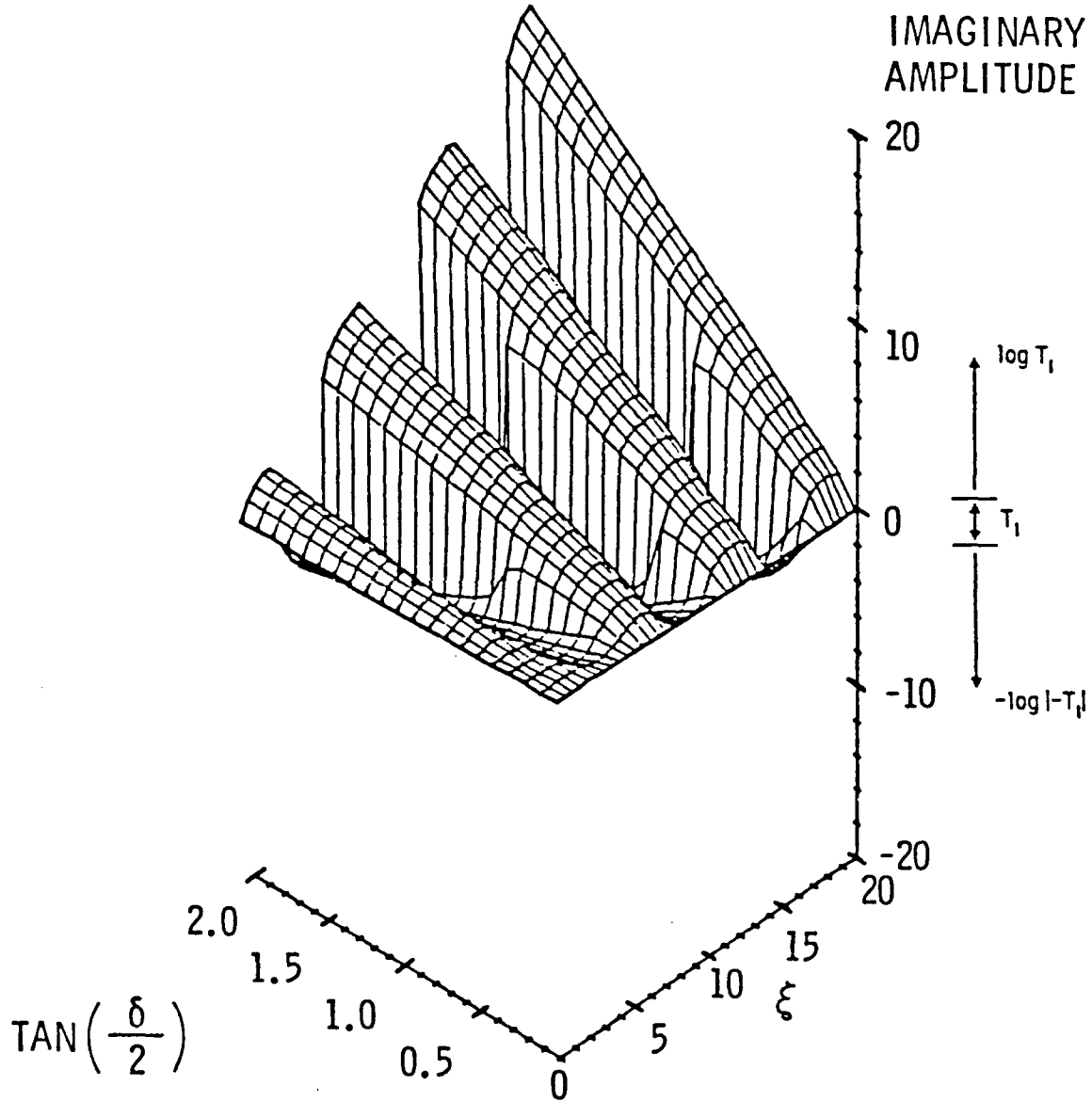

Figure 2.2 Three-Dimensional Grid Plot of the Imaginary Transfer Function Amplitude as a Function of ξ and tan(δ/2) or an Assumed Mass Ratio R= 1.0.

values of the negative values less than -1 are plotted as negative numbers, and the values between 1 and -1 are plotted directly.

Undulations in the plots are analogous to the modes of the mass-loaded rod. Notice that the real and imaginary plots are out of phase in the sense that a peak of one curve nearly corresponds to a zero of the other curve. The zeroes of the real transfer function amplitude indicate the locations of the resonances. The zeroes of the imaginary transfer function amplitude indicate the locations of the antiresonances.

The plots of the real and imaginary transfer function amplitudes in Figs 2.1 and 2.2 show only the positive ξ and $\tan(\delta/2)$ axis values. Convergence to negative values can be achieved, but would result in negative loss factors and storage moduli, neither of which have any physical meaning.

The benefit of seeing the transfer function plots is that the regions of convergence can be accurately located. The trick is to turn this visualization into a solution algorithm. Another variable complicates the problem. Equations (2.2) and (2.3) are functions of three variables: ξ, Ω, and R. The effect of increasing R will be to shift the undulations down the ξ axis.. This corresponds to the shift in resonances when the end mass is changed. Any "seed" generating algorithm would have to consider the interrelationship between all three variables and the mode number.

Fortunately, the transfer function equations are very nearly independent of the damping parameter, $\tan(\delta/2)$, for a given frequency parameter, ξ. The modes are almost uniformly separated along the ξ axis by the value π. It is

only for small values of damping that the damping parameter becomes a strong function of ξ.

Using the above properties, it would not be difficult to program a seed algorithm to locate the approximate values of ξ by assuming a value for $\tan(\delta/2)$ and solving for ξ knowing the value of R. However, this would require too much computer time and the seed values would still be approximate because $\tan(\delta/2)$ is approximated. In addition, this same iteration procedure would need to be repeated at each frequency.

A seed generation routine which is just as accurate yet employs much less computer time is a two step polynomial curve fitting procedure which locates seed values quickly and accurately, usually within 5% of the true solution. Two curves are necessary. The first polynomial curve locates the approximate ξ value for the first mode as a function of R. A plot of the relationship between ξ and R for the first three modes can be seen in Fig. 2.3. The equation used in this study to approximate the curve for mode 1 is:

$$\xi_1 = .002R^2 - .132R + 1.254 \qquad (2.19)$$

The quantity $\tan(\delta/2)$ is assumed to be equal to 0.1. Even if the true value of $\tan(\delta/2)$ is 0.01, the ξ values for the first mode will only differ by 0.1% from the ξ values computed with $\tan(\delta/2)$ equal to 0.1.

Once the true value of ξ_1 is obtained, it can be used in the second polynomial curve fitting procedure to approximate the higher mode seed values. This polynomial curve is based upon the ξ versus n (mode number) plot being a straight line at higher frequencies with a slope very near π.

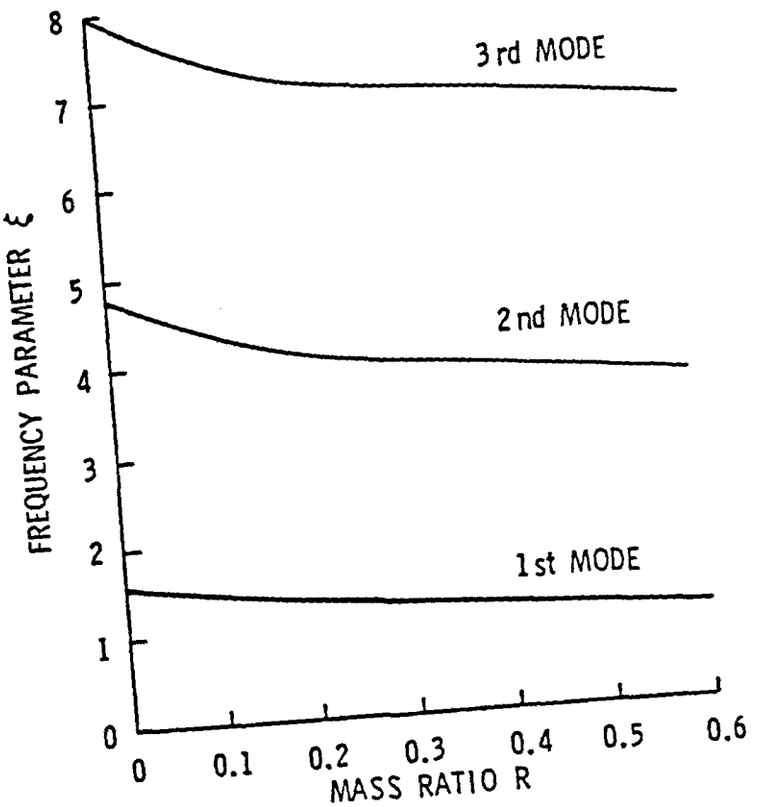

Figure 2.3 Frequency Parameter, ξ, as a Function of the Mass Ratio, R, for $\tan(\delta/2) = 0.1$.

The plot in Fig. 2.4 shows that this is indeed the case. The mass ratio, R, is assumed to be equal to 1.0 for this plot. Different values for R will not significantly alter Fig. 2.4. Notice that the curve only shifts appreciably for very high damping values, yet the slope still remains the same as that for the lower damping curves. Thus, knowing the first mode value for ξ and the approximate slope, it should be simple to find ξ for the higher modes. The simple, yet effective, equation used to approximate ξ_n for higher modes is:

$$\xi_n = (n-1)\pi + \xi_1/n \qquad (2.20)$$

Again, the ξ values are the more important of the two variables (ξ,Ω) in the transfer function equations since the damping parameter can roughly be considered independent of frequency. By applying a window on the convergence limits about this seed, the correct solution can be assured barring discontinuities in the amplitude and phase data.

The key to improving the solution method is that once the solutions for the resonance and antiresonance frequencies are obtained accurately, it is a simple matter to use linear interpolation between adjacent modes to find solutions at any frequency providing the frequency lies between two modes whose solutions have been determined. This scheme was employed in the current study to obtain results across the entire frequency range of interest instead of only solving for η and E' at the $\pm 90^\circ$ transfer function phase points.

Another improvement made in this study, which has been overlooked by many investigators, is the use of the lateral vibration correction as derived

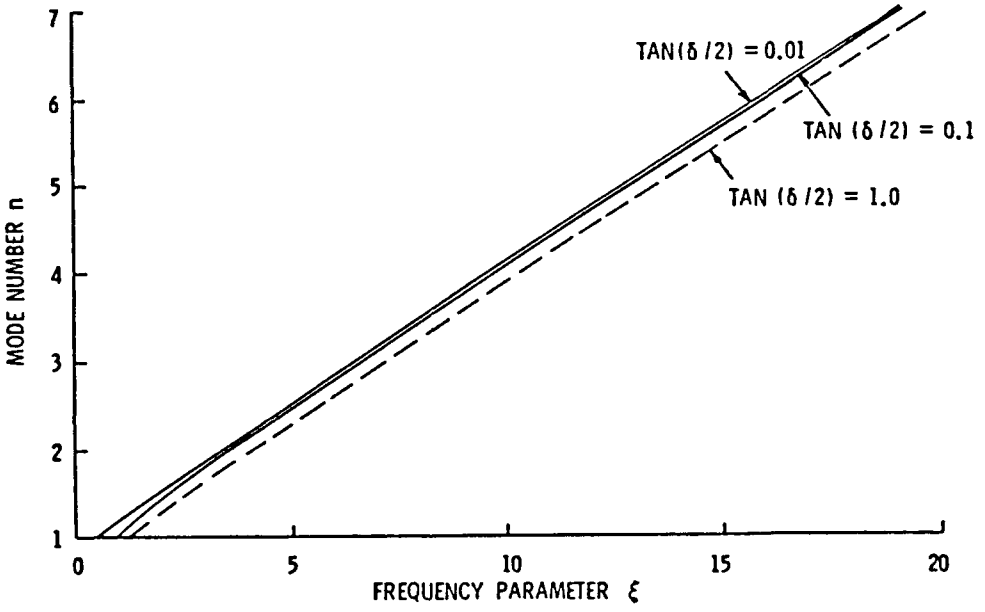

Figure 2.4 Mode Number Versus the Frequency Parameter, ξ, at Different Damping Levels for Mass Ratio, R= 1.0.

by Pritz [24]. Equations (2.13) and (2.14) were incorporated into the solution algorithm to improve the accuracy of the results. The assumption, as discussed by Snowdon [9], that Poisson's ratio can be considered a real value ($\eta_v = 0$) for plastics and rubbers was also assumed for this study.

CHAPTER 3

EXPERIMENTAL PROCEDURE

3.1 Equipment Setup

The Transfer Function Method is particularly amenable to the use of accelerometers for recording vibration levels. In most tests the accelerometer signals must be calibrated and the vibration source must have a feedback control to monitor the vibration levels. Neither is required with the Transfer Function Method since only the relative acceleration levels are needed. If the two accelerometers attached at the ends of the test sample are well matched over the frequency range of interest, their output voltage ratio will be equal to the acceleration ratio. In addition, any variations in the input acceleration level from the shaker will not hamper the test as the response of interest is the ratio between the accelerations of the two ends of the sample.

The equipment setup used in this study is shown in Fig. 3.1. A bar-like sample is harmonically vibrated along its axis, at the frequency of interest, by an Electrodyne Shaker. Two BBN 501 Accelerometers, mounted on either end of the sample, supply a voltage signal proportional to the acceleration. Each signal is then amplified before feeding into a HP 3570A Network Analyzer. The Network Analyzer digitizes and filters the signals before computing the relative amplitude and phase between the two inputs.

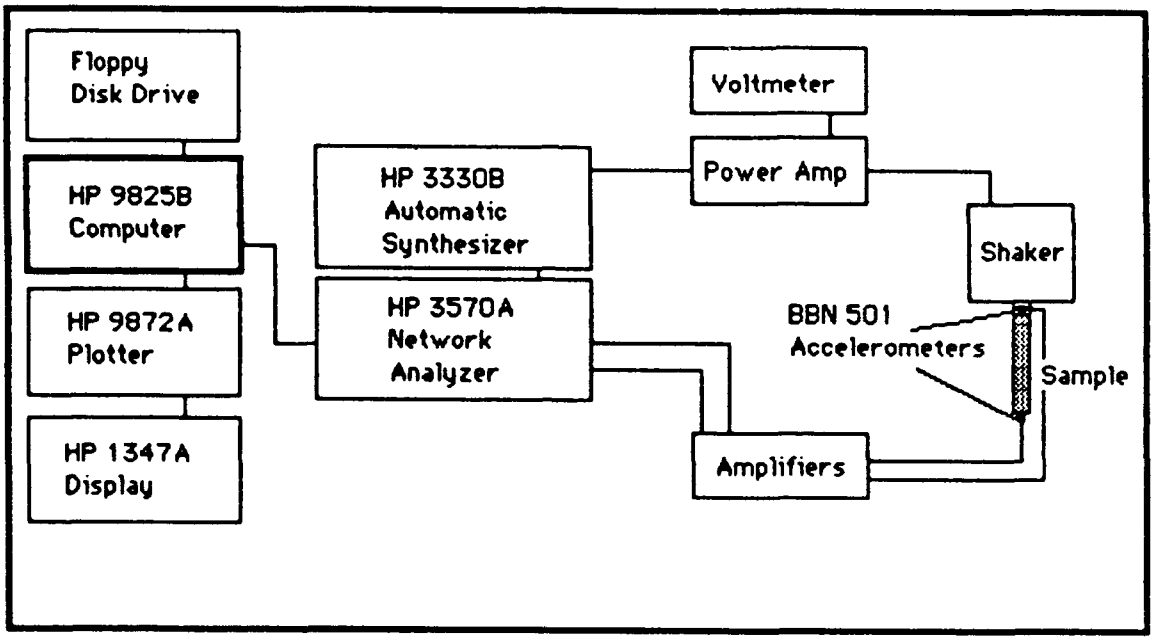

Figure 3.1 Equipment Setup for Transfer Function Method Tests.

The shaker is driven by a HP 3330B Automatic Frequency Synthesizer. The HP 3330B communicates to the HP 3570A via an interface bus (HP 1B). This provides the HP 3570A with the input frequency on which to perform the bandpass filtering. The filter bandwidth used in this study was 10 Hz.

The entire test setup is controlled by a HP 9825B computer/controller through the same interface bus. The HP 9825B also performs all of the numerical calculations, stores all the data on floppy disks, and controls both a display monitor and pen plotter so that plots of the results can be made. A thermal printer outputs the test results in tabular form during the testing. The computer, display, and pen plotter are shown in Fig. 3.2.

The shaker-specimen fixture, as shown in Fig. 3.3, is a brass tripod with neoprene gaskets to reduce lateral structure-borne vibration. The fixture is small enough to fit inside a Tenney Temperature Chamber should tests at various temperatures be desired. The sample is connected to the shaker by a small rectangular brass stirrup which threads into the shaker. One of the accelerometers is mounted inside this stirrup while the other accelerometer is attached to a brass end mass. To permit magnetic materials to be tested, such as the NEC Composite, brass was used to make many of the test fixture components because it is a nonmagnetic metal.

Two types of epoxy were used in the study. The accelerometers were each cemented to their respective brass fixtures with a fast-setting cyanoacrylate ester adhesive called Loctite Super Bonder 495. This type of adhesive is similar to the "super glues" popular a few years ago. The

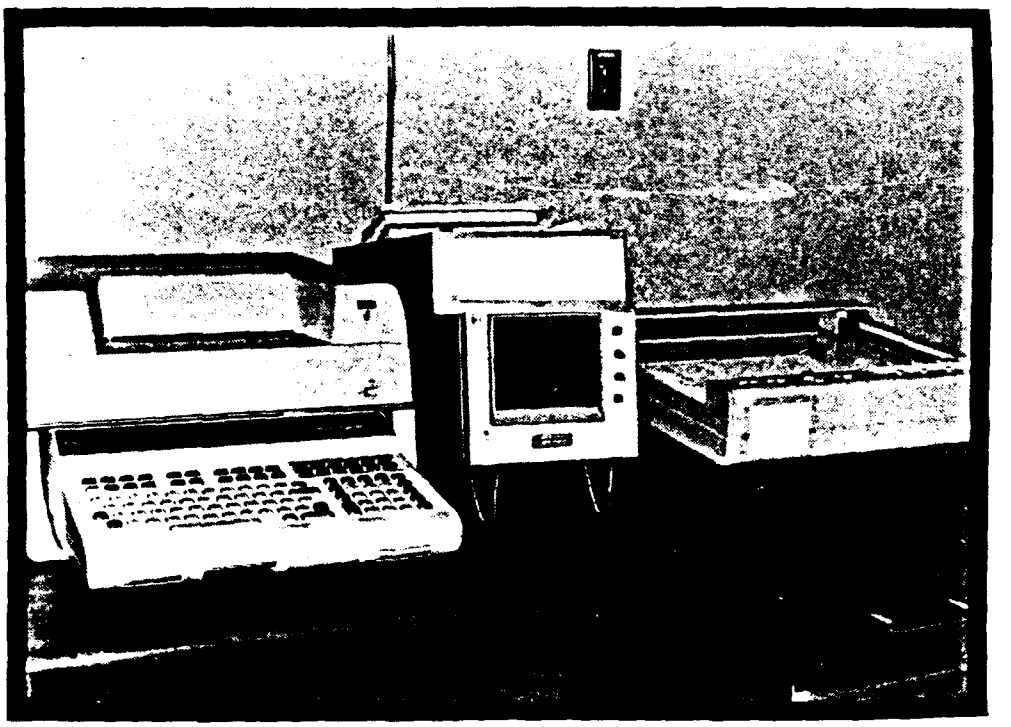

Figure 3.2 HP 9825B Calculator, HP 1347A Display Monitor, and HP 9872A Pen Plotter.

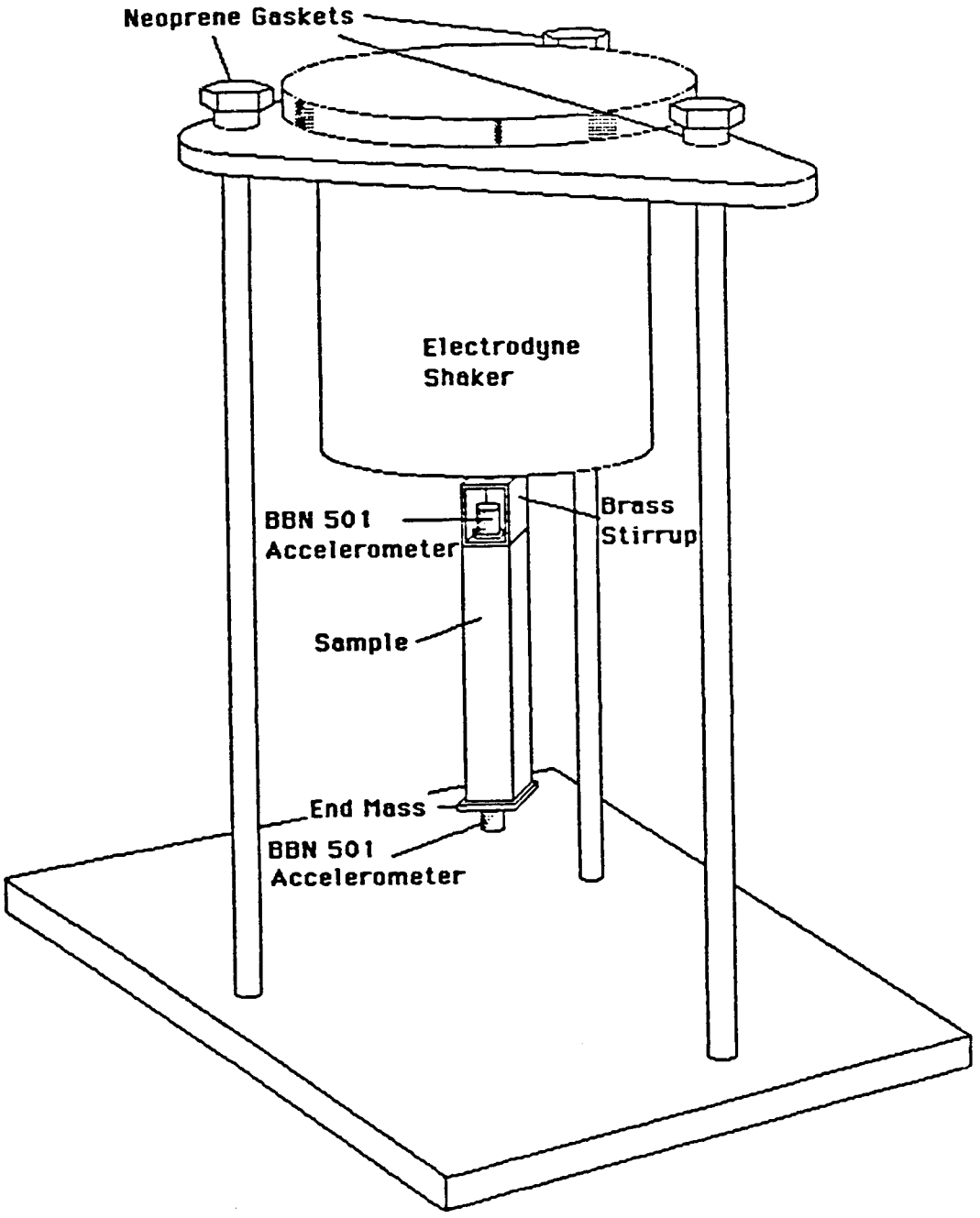

Figure 3.3 Tripod Shaker-Specimen Test Stand.

sample-brass interface was sealed using a quick-setting epoxy sold under the trade name Epoxi-Patch by the Dexter Corporation. The Epoxi-Patch adhesive hardens to an extremely brittle compound within 5 to 10 minutes. These properties made it ideal for this study since it did not require a long curing period and the hardened epoxy could be chipped off the relatively soft samples without tearing or otherwise damaging them.

The Network Analyzer and Frequency Synthesizer are extremely accurate. The Network Analyzer is accurate in amplitude measurements to 0.4 dB and accurate to 0.2° in phase measurements over the frequency range of the tests. Both of these errors are far below the error of the rest of the electronic equipment and the error associated with poor mounting of either the accelerometers or samples.

The rest of the equipment setup was tested to ensure that the accelerometer signals were well-matched and not distorted by any differences in the signal channels. First the accelerometers were mounted side-by-side on a fixture attached to the shaker. The response of each accelerometer was recorded on a dB scale with 1.0 volt as the reference. Figure 3.4a shows these two signals on the same plot. They match very well over the frequency range of interest considering that they were mounted to a thin plate at slightly different locations. Figure 3.4b is a comparison of the same input accelerometer signal fed through the two measurement channels. The signals compare so well that it is difficult to discern two separate curves. This ensures that both channels of the power source and

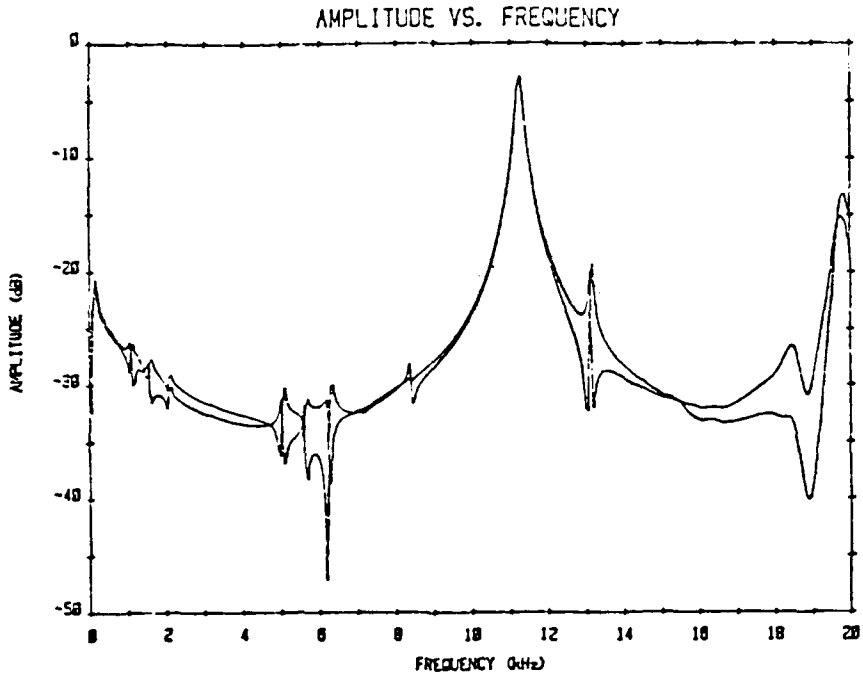

Figure 3.4a Response of Each Accelerometer When Mounted Side-By-Side to a Fixture Attached to the Shaker. (Reference=1.0 volt)

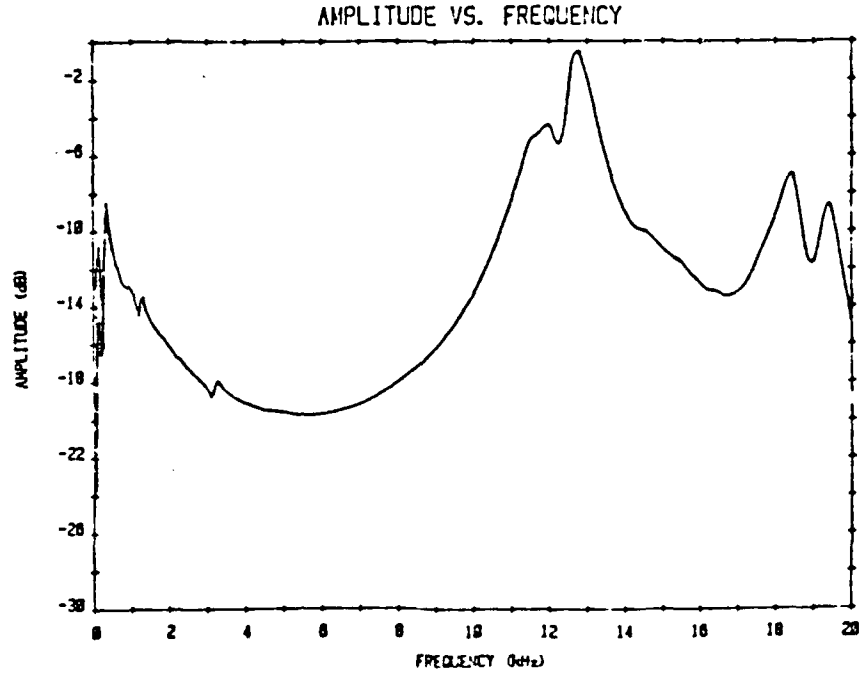

Figure 3.4b Response of an Accelerometer Signal Passed Through the Two Channels. (Reference= 1.0 volt)

preamplifier are well-matched.

3.2 Materials Tested

The twelve materials tested in this study are listed in Table 3.1. The first seven consist of PZT ($PbZrTiO_3$) or TiO_2 powder embedded in a polymer matrix. These composites are classified as 0-3 composites. This indicates that the PZT particles are completely encapsulated within the polymer matrix. The 0 denotes no connectivity in any direction for the filler while the 3 indicates that the polymer possesses connectivity in all three directions. The primary reason for using PZT in the compounds instead of a less expensive, dense powder, such as lead, is that PZT may provide additional damping due to electromechanical losses. A comparison between PZT polymer composites which have been polarized and the same unpolarized composites should reveal the extent of the additional damping, if any, caused by electromechanical dissipation.

One sample tested consisted of anatase (TiO_2) in a polypropylene matrix. Anatase has a similar morphology to PZT except that it cannot be polarized. Loss factor differences between an anatase-polymer composite and a PZT-polymer composite of the same polymer and volume percentage of filler might indicate that even an unpolarized piezoelectric material contributes some amount of electromechanical damping.

The amount of PZT embedded in the polymers varied from 0 to 60% of the volume fraction. Some duplicate samples, fabricated at different times,

Table 3.1 - Materials Tested and their Manufacturers

Material	Manufacturer
$PbZrTiO_3$ (PZT501A)	Ultrasonic Powders
TiO_2 (Anatase)	Whittaker Clark Daniels
Polyethylene (Marlex 6001)	Phillips Petroleum
Polypropylene	Phillips Petroleum
Polychloroprene	Polysciences
Spurrs epoxy	Polysciences
Eccogel (Eccogel Zero)	Emerson & Cumming
Polyurethane (EN-4)	Conap
Neoprene (GN 35003)	B. F. Goodrich
NEC Composite	Nippon Electric Company
SOAB	B. F. Goodrich
Aluminum (6061)	Unknown

were made to provide an indication of the variability between two batches of the same composite.

The materials tested in this study were fabricated at the Materials Research Laboratory, on the campus of The Pennsylvania State University, as part of a related research project to characterize various properties of ferroelectric/ferromagnetic polymer composites. Two separate procedures were used to form the composites [26].

The polyethylene and polypropylene composites were made using the following procedure. First the PZT powder was sieved using a No. 325 mesh (particle size less than 45 microns). Next, the PZT and polymer were mixed together using a Brabender mixer at 40 rpm for 20 minutes. After mixing, the materials were hot pressed at pressures ranging from 5000 to 10000 psi. The temperature used during this operation was 160°C for the polyethylene and 195°C for the polypropylene. The final step was to cool the samples to room temperature while still under pressure.

A similar procedure was followed for the Eccogel and Spurrs epoxy composites. The PZT powder was sieved using the same No. 325 mesh. The PZT was mixed with the polymer using either the Brabender or, in the case of the Eccogel composites, by adding the PZT to the liquid polymer. The next stage was to pour the mixture into a Teflon mold and sonicate it to remove air bubbles. The mixture was then cured at 70°C for 8 hours.

Some of the materials tested cannot be considered purely viscoelastic since PZT, an elastic material, is used as a filler. Thus, the dynamic

modulus of the PZT composites should not be as strong a function of frequency or temperature as that of the pure polymers.

The PZT was not polarized in any of the samples tested. Samples will be poled at a later date due to difficulties in polarizing the present composites. This difficulty was primarily due to the low conductivity of the polymers. The addition of carbon black to the composites was being considered at the time of this thesis.

3.3 Dynamic Modulus Computer Program

The computer program used to run the test apparatus and solve Eqs. (2.2) and (2.3) for the loss factor and storage modulus was written in HPL (Hewlett Packard Language). HPL is a simple form of BASIC with short commands and single letter variables. It is primarily a scientific language which performs very well and has an extensive error recovery system, but does not allow easy interpretation due to the lack of meaningful variable names available in most computer languages. For example, instead of using "LOSFAC" to represent the loss factor, the array "D" is used. For this reason it is felt that a more instructive description of the program can be achieved by using the flowchart in Fig. 3.5. than by including a copy of the program listing.

The entire program consists of four sections: parameter input, search for resonances, solution of the equations, and data storage/retrieval. The first stage of the program interactively loads the necessary material

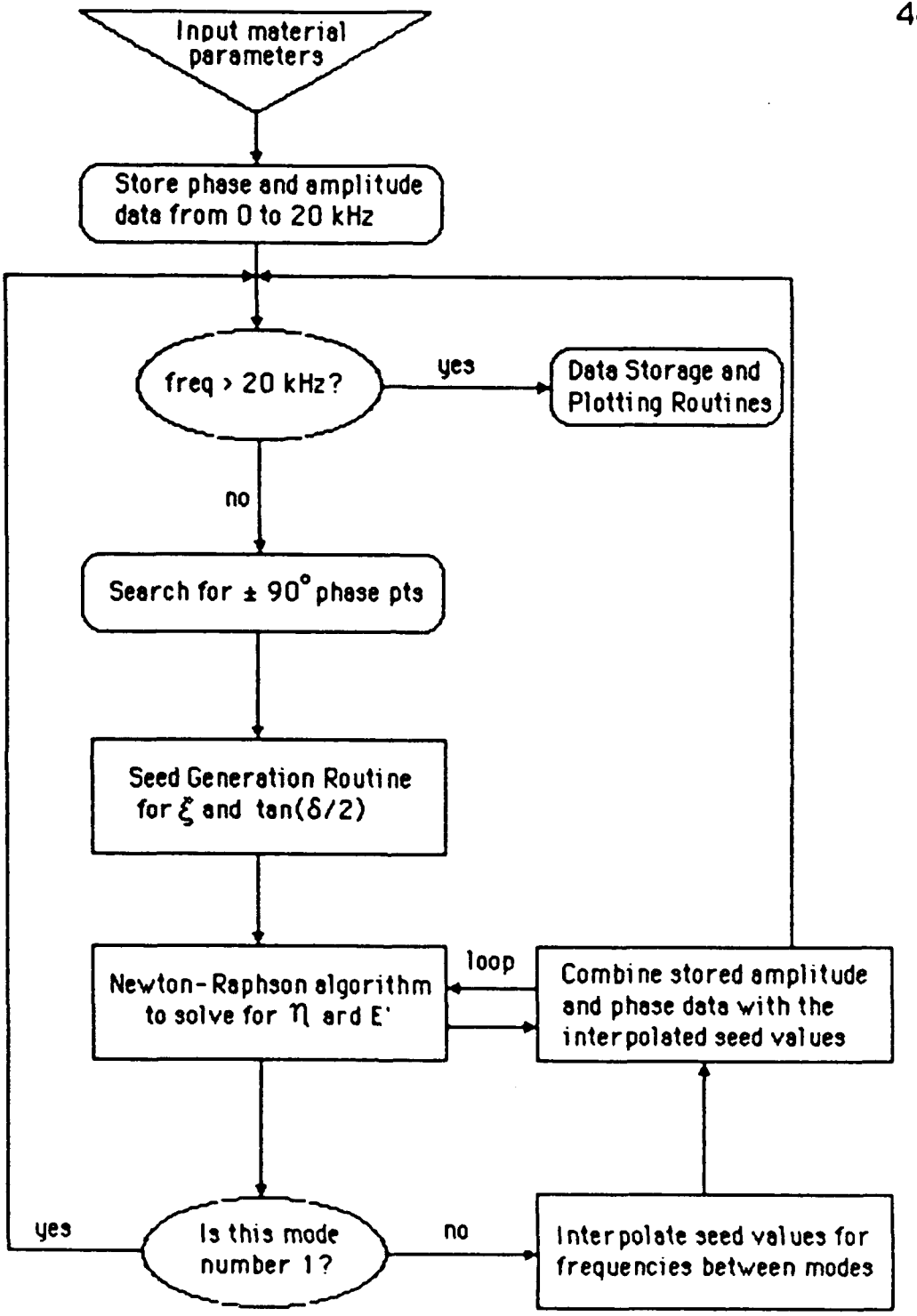

Figure 3.5 Computer Flowchart of Program Used to Compute the Loss Factor, η, and Storage Modulus, E'.

parameters. After these are loaded, the phase and amplitude values, measured at frequency increments of 50 Hz, are saved in an array for use later. The primary resonance is also located during this initial search and array-loading operation. Knowing the approximate frequency of the first mode saves a great deal of time during the "search" stage.

The search for the ± 90° phase points is the next step. The method of searching is iterative. Phase values are read until the ± 90° point is passed. The frequency step is decreased and the search begins at the last frequency read before passing the resonance. In this manner the resonance frequencies can be ascertained to within 0.1 Hz.

Once the resonance is located, the phase, amplitude and frequency values are used as input to the solution algorithm. Before beginning the solution process the seed values ξ and Ω are determined using the procedure discussed in Chapter 2. The next step is to use the Newton-Raphson solution technique along with Eqs. (2.2) and (2.3) to solve for the loss factor and storage modulus. If this is not the first mode then the results for frequencies between this mode and the previous one are determined by using the values for ξ and Ω at the two modes to interpolate the seed values for the frequencies between these two resonances. The data stored in 50 Hz increments at the very beginning are used along with the Newton-Raphson solution technique to find η and E' at frequencies between the modes.

This same procedure is repeated for the remaining modes until the frequency exceeds 20 kHz or one of the accelerometer outputs reaches the

noise limit of the equipment. Since the driven end accelerometer signal does not vary appreciably with different samples, the amplitude ratio corresponding to the noise floor can be estimated. This value is usually near -70 dB. The program also contains an option to extrapolate seed values past the last mode and solve for E' and η for frequencies up to the 20 kHz limit. The upper frequency limit of 20 kHz was chosen based upon the assumption that the epoxy bond could not be considered truly rigid at higher frequencies.

The results are then stored onto a floppy disk so that they may later be retrieved, edited, or appended. Several different plotting routines are also linked with the program. The amplitude and phase data from the test can be plotted versus frequency to determine if there are any problems with equipment malfunctions or if the sample is improperly mounted. These plots can also be used to find the frequency at which the noise level of the accelerometer signals is reached. The noise level is characterized by random fluctuations in both the phase and amplitude plots. Typical plots of the amplitude and phase can be seen in Figs. 3.6a and 3.6b. The material tested is polyurethane. Most materials are characterized by only two or three modes in this frequency range instead of the six shown here.

Several plotting routines exist for displaying the loss factor, the storage modulus, or both. The particular plotting routine used contains an option to fit a least squares polynomial curve through the data if desired.

The dynamic modulus testing procedure has been almost totally

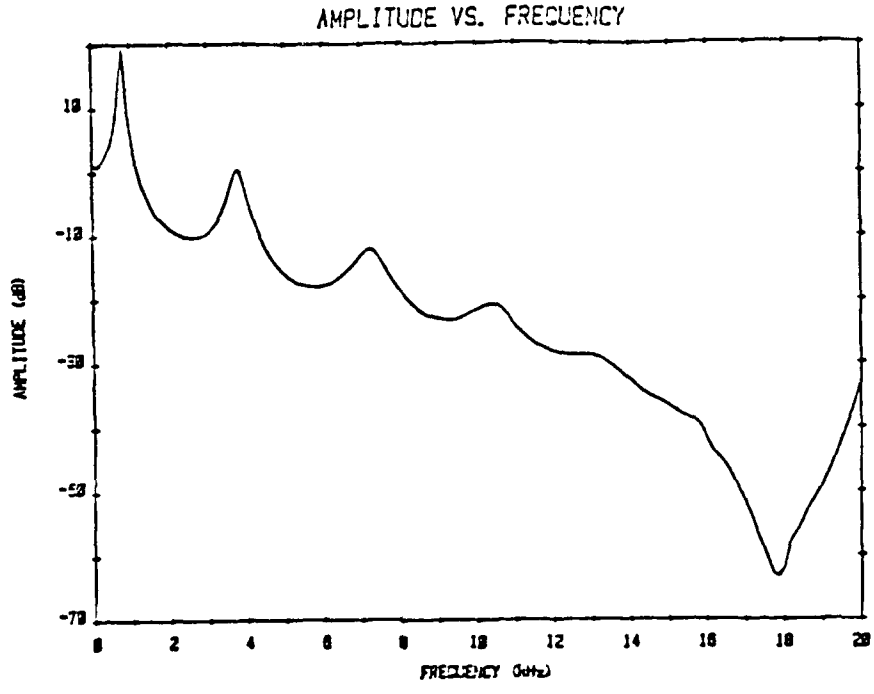

Figure 3.6a Amplitude of Acceleration Ratio Between the Mass-Loaded End and the Driven End of a Rod-Like Specimen.

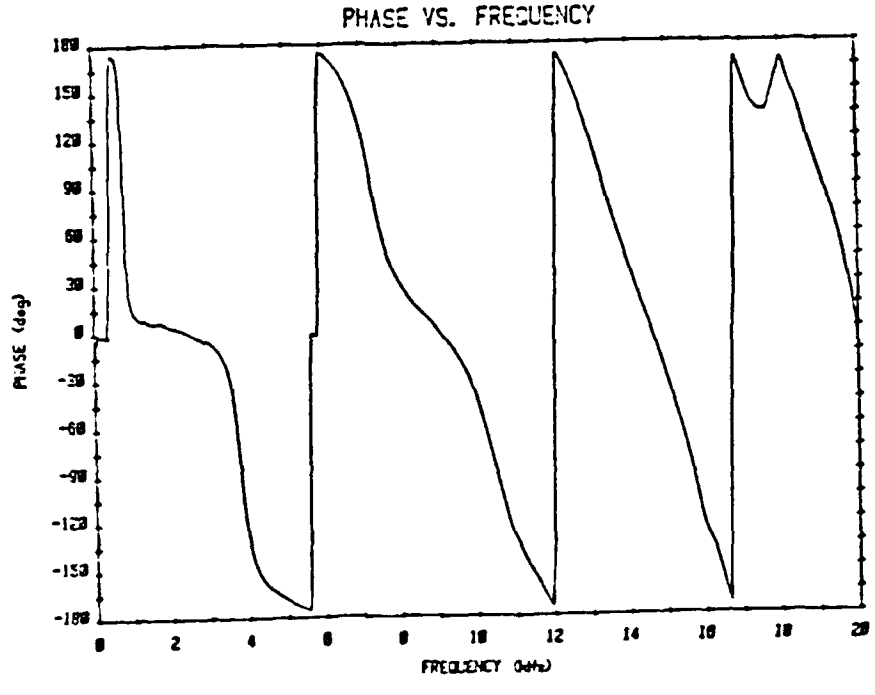

Figure 3.6b Phase of Acceleration Ratio Between the Mass-Loaded End and the Driven End of a Rod-Like Specimen.

automated. The input material parameters are entered into the computer and ten minutes later a plot of the loss factor and storage modulus can be obtained.

CHAPTER 4

DISCUSSION OF RESULTS

4.1 Introduction

The results are presented in the form of plots of both the loss factor and storage modulus versus frequency. The ordinate axes are individually scaled to make maximum use of the plot area. The abscissa (frequency axis) is not scaled and thus some of the plots only contain data for the initial portion of the frequency interval.

The samples were all approximately 7 to 8 cm in length and 1 cm^2 in cross-sectional area. The corrections for the shape factors, as computed using Eq. (1.3), were negligible. All tests were performed at room temperature, 24°C. In order to combine results taken using different end masses at different times, the temperatures had to be the same. The ambient room temperature was chosen because it was fairly constant. In addition, tests were attempted at temperatures ranging from -20°C to 45°C but the available Tenney Temperature Chamber could not provide a stable temperature for the duration of any test. The composites containing 25% or more PZT by volume could not be considered true viscoelastic materials and thus application of the time-temperature superposition principle would have been inaccurate for these samples. Note again that in no case were the PZT particles polarized, i.e. they function simply as rigid particles added to

the polymer matrix material. The results are grouped according to the polymer matrix of the composites.

4.2 Eccogel Composites

The composites composed of PZT and Eccogel presented some difficulties during the testing procedure. Eccogel is extremely compliant; it has a consistency close to gelatin. It molds very easily, but tends to contort upon setting. Results for frequencies higher than 5 kHz were difficult to obtain for the Eccogel composites because the acceleration levels of the mass-loaded end approached the electrical noise limit of the equipment.

In spite of these difficulties, the test results appear good. The first plot, shown in Fig. 4.1, details the loss factor and storage modulus results of Eccogel without the addition of PZT. As might be expected, with a very compliant material, the damping is high. The loss factor peak, corresponding to the region of transition between the "rubbery" stage and the "glassy" stage (see Fig. 1.1) of the material, occurs at 1.8 kHz. The storage modulus increases over the entire frequency range.

The addition of PZT to the Eccogel reduces the loss factor values and increases the storage modulus. The addition of a ceramic, such as PZT, will always tend to increase the storage modulus of a less rigid polymer. Figures 4.2a and 4.2b contain dynamic modulus results for identical Eccogel samples containing 10% PZT by volume. The term "identical" is used here to

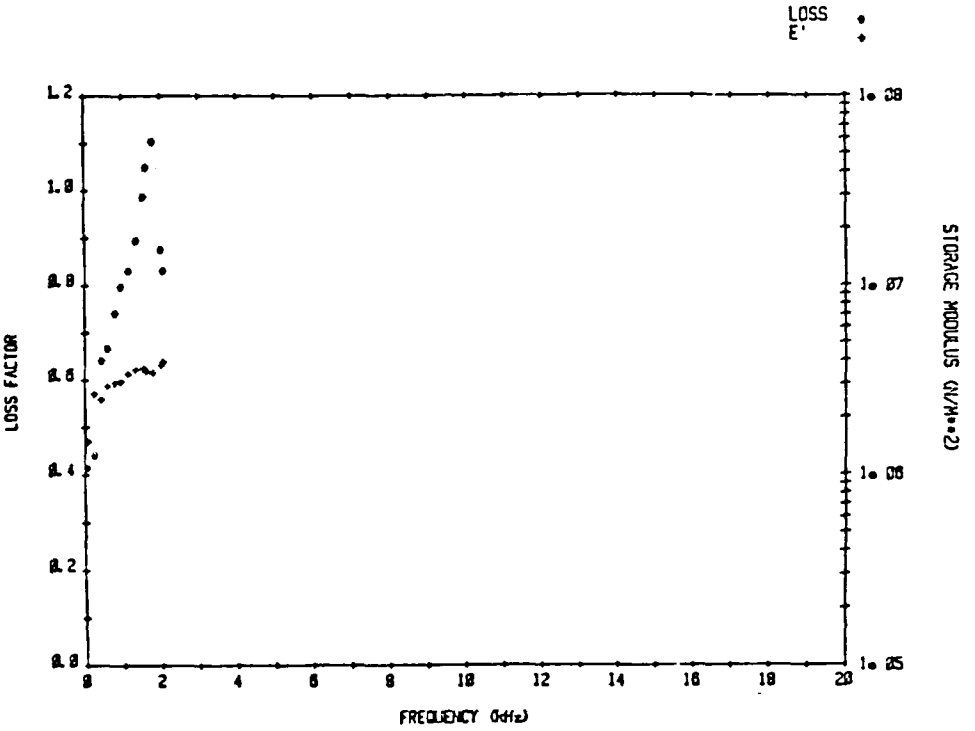

Figure 4.1 - Loss Factor and Storage Modulus Versus Frequency for an Eccogel Sample.

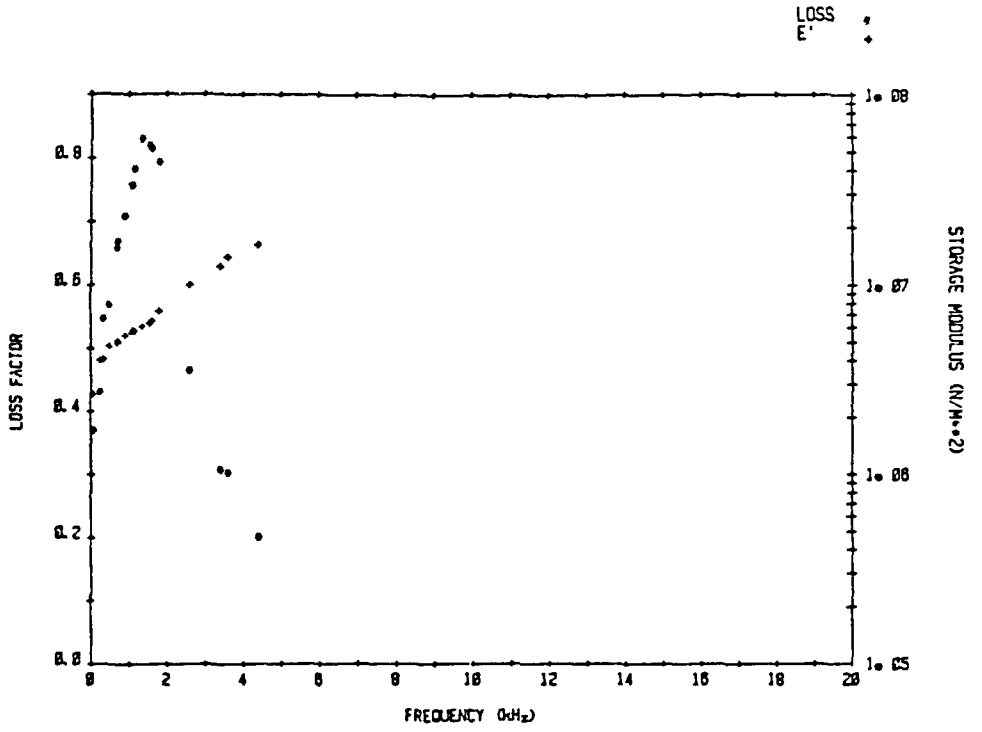

Figure 4.2a - Loss Factor and Storage Modulus Versus Frequency for an Eccogel/10% PZT Sample (No.1).

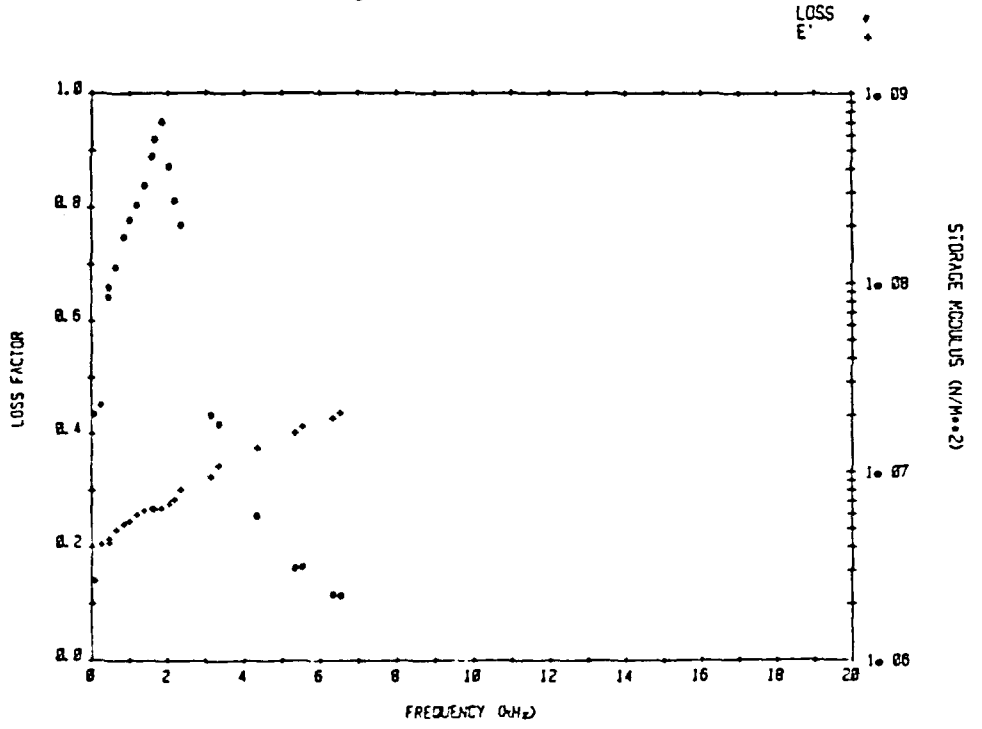

Figure 4.2b - Loss Factor and Storage Modulus Versus Frequency for an Eccogel/10% PZT Sample (No. 2).

indicate that the composites contain the same proportion of polymer and filler. However, slight variations in the fabrication process may cause "identical" samples to possess different mechanical properties. While the general trends of the loss factor curves are similar, Fig. 4.2b displays slightly higher damping. The loss factor peaks at approximately the same frequency as the pure Eccogel sample. The storage modulus curves for the two materials agree well.

The addition of more PZT, 25% by volume, increases the storage modulus by a factor of 5 over Eccogel alone. The plots of the dynamic moduli of identical samples are shown in Figs. 4.3a and 4.3b. The loss factor curves differ from those previously shown. Initially the loss factors decrease but then increase without reaching a peak. This same pattern is repeated for many of the specimens containing other polymers.

4.3 Polyethylene Composites

The composites made using polyethylene as the matrix material generally have low damping properties compared to the Eccogel samples (an order of magnitude lower). A plot of the loss factor and storage modulus of undoped polyethylene, Fig. 4.4, shows a gap where no results are available. These results were discarded because they were deemed to be unreliable. When the phase angle of the transfer ratio is close to 0° the correct solution of Eqs. (2.2) and (2.3) becomes very difficult to obtain. This was discussed in detail in section 2.2.1. The loss factor curve in Fig. 4.4 most

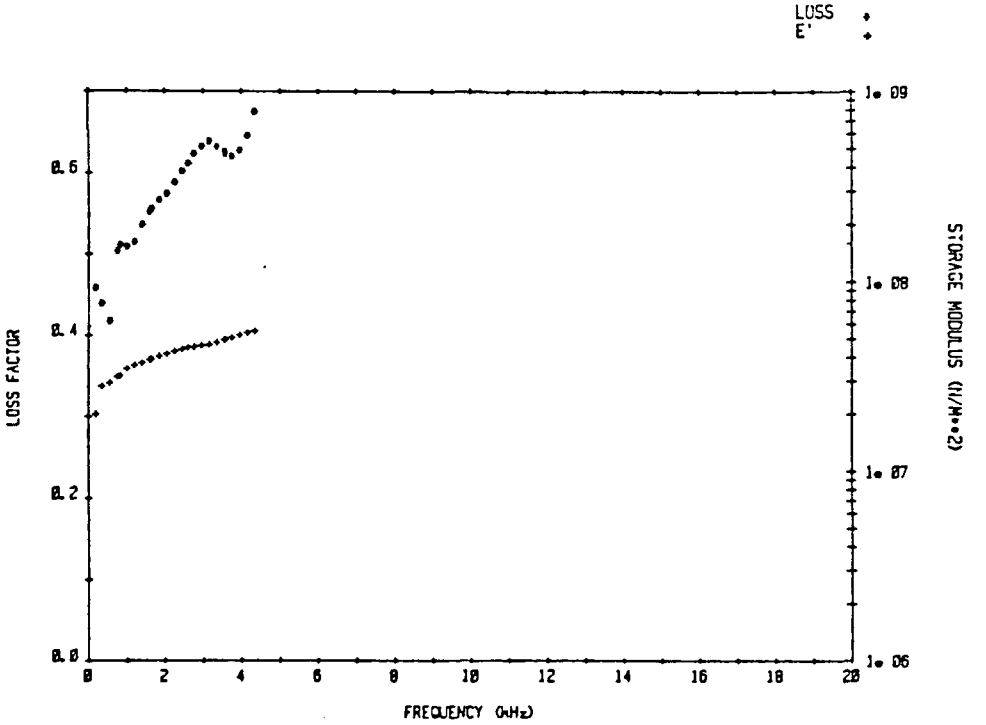

Figure 4.3a - Loss Factor and Storage Modulus Versus Frequency for an Eccogel/25% PZT Sample (No.1).

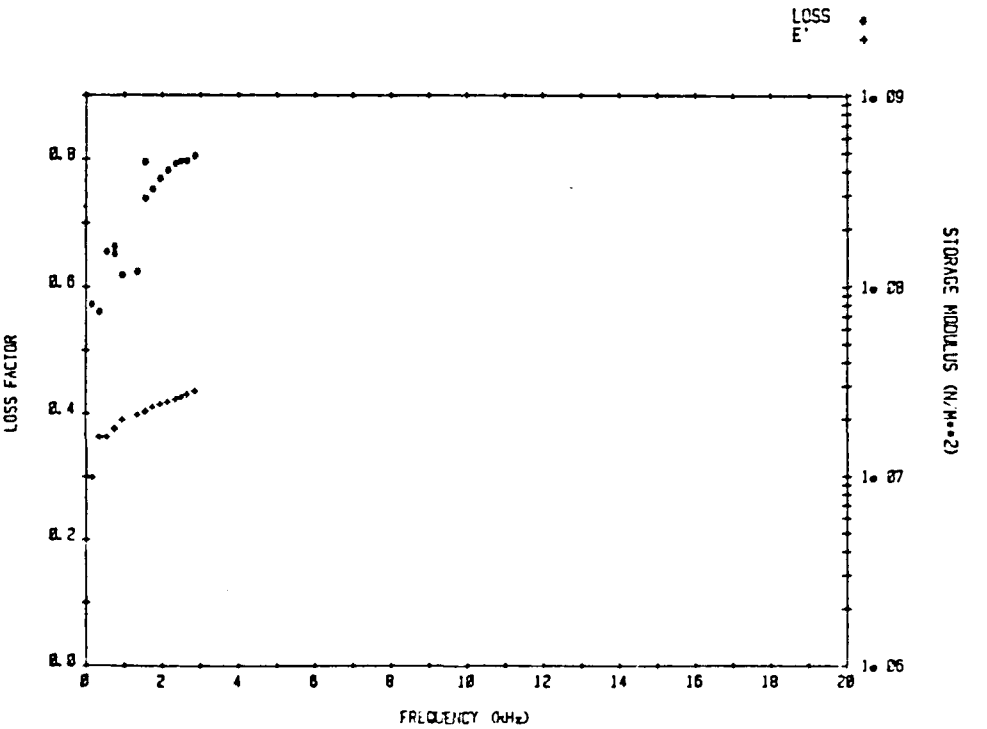

Figure 4.3b - Loss Factor and Storage Modulus Versus Frequency for an Eccogel/25% PZT Sample (No. 2).

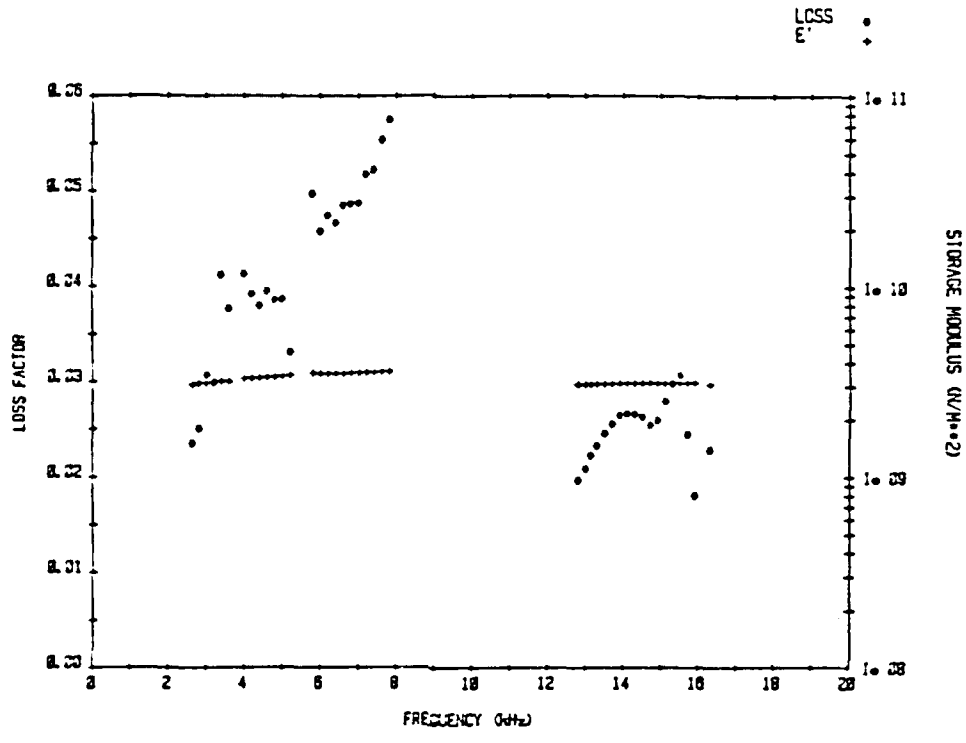

Figure 4.4 - Loss Factor and Storage Modulus Versus Frequency for a Polyethylene Sample.

likely peaks near 9 kHz and then decreases in value until it reaches the data points at 12 kHz.

Figures 4.5a and 4.5b contain the results for identical specimens of 25% PZT and polyethylene. Again, the addition of PZT increases the storage modulus. There is a fairly wide scatter in the results for the loss factor in both plots. In the first plot a peak appears to occur near 8 kHz. Unfortunately, the second plot contains no results at this frequency to either confirm or deny the existence of a peak. The regions containing no data points signify frequencies where the phase of the transfer ratio is very close to 0°.

A discrepancy exists in the loss factor values for frequencies greater than 15 kHz. In Fig. 4.5a, the loss factor increases for higher frequencies while in Fig. 4.5b it remains stable over the same region. This indicates that either the material or some aspect of the test setup was different. This phenomenon of increasing loss factor also occurs in the plots of other tests with different materials.

Two possible mechanisms might account for the rapid increase in damping for the first polyethylene sample with 25% PZT (Fig. 4.5a). One explanation could be that the epoxy holding the sample to the test fixture became ineffective at the higher frequencies and caused an increase in friction at the epoxy-specimen interface. This would explain why Fig. 4.5b did not show the same loss factor pattern. Unfortunately, a second test

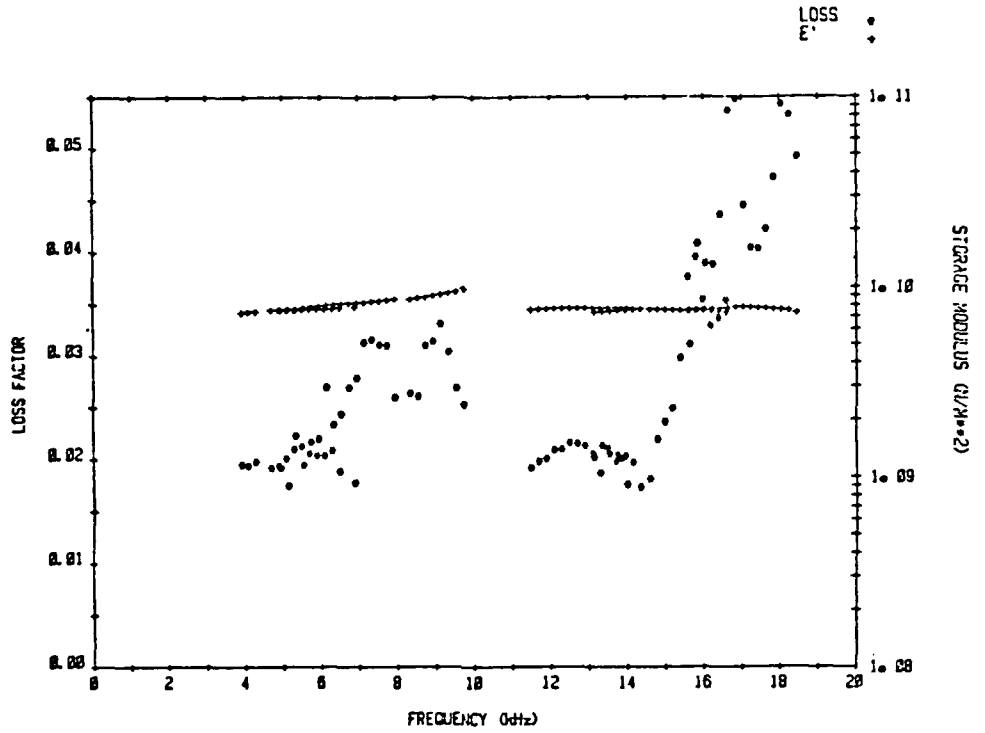

Figure 4.5a - Loss Factor and Storage Modulus Versus Frequency for a Polyethylene/25% PZT Sample (No.1).

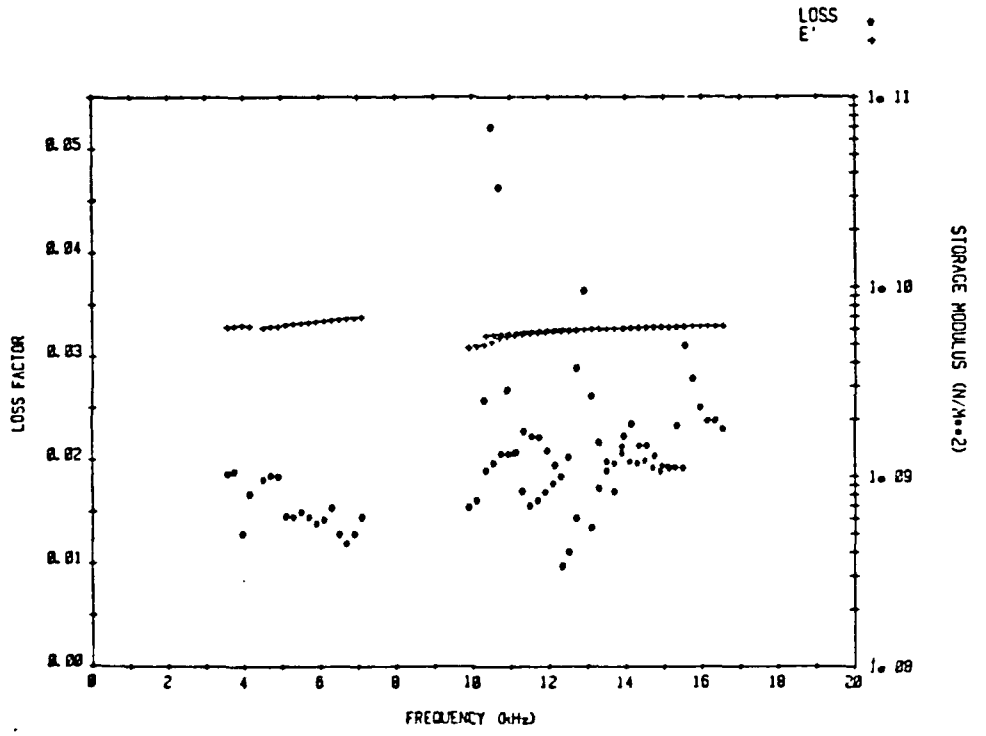

Figure 4.5b - Loss Factor and Storage Modulus Versus Frequency for a Polyethylene/25% PZT Sample (No. 2).

using the sample from Fig. 4.5a was run and the test results match the first results fairly well; notice that two separate storage modulus lines can be seen on each plot. A second possibility is that the sample in Fig. 4.5a was more porous than the sample, of the same composition, shown in Fig. 4.5b. Variations in the mixing duration of the polymer and filler could account for this difference. Damping, in the form of friction, is generated by the expansion-compression cycle of the pores. The same effect occurs if the material contains voids. This would explain the increased damping at high frequencies for one sample as compared to the relatively stable damping of a second sample.

Figure 4.6 contains the loss factor and storage modulus results for a 60% PZT and polyethylene composite. This was the most dense sample tested (4.75 g/cm^3). The storage modulus curve is somewhat flat and approximately twice the value of the 25% PZT composites. A sharp peak in the loss factor occurs at approximately 15.6 kHz. It is possible that increasing the density shifts the rubbery frequency range to a higher value and causes a more narrow loss factor peak.

4.4 Polypropylene Composites

No samples with PZT were available using polypropylene as the matrix material. The two plots shown in Figs. 4.7a and 4.7b contain the dynamic modulus results for a pure polypropylene specimen and a polypropylene and 25% anatase specimen. The damping for the polypropylene is fairly high and

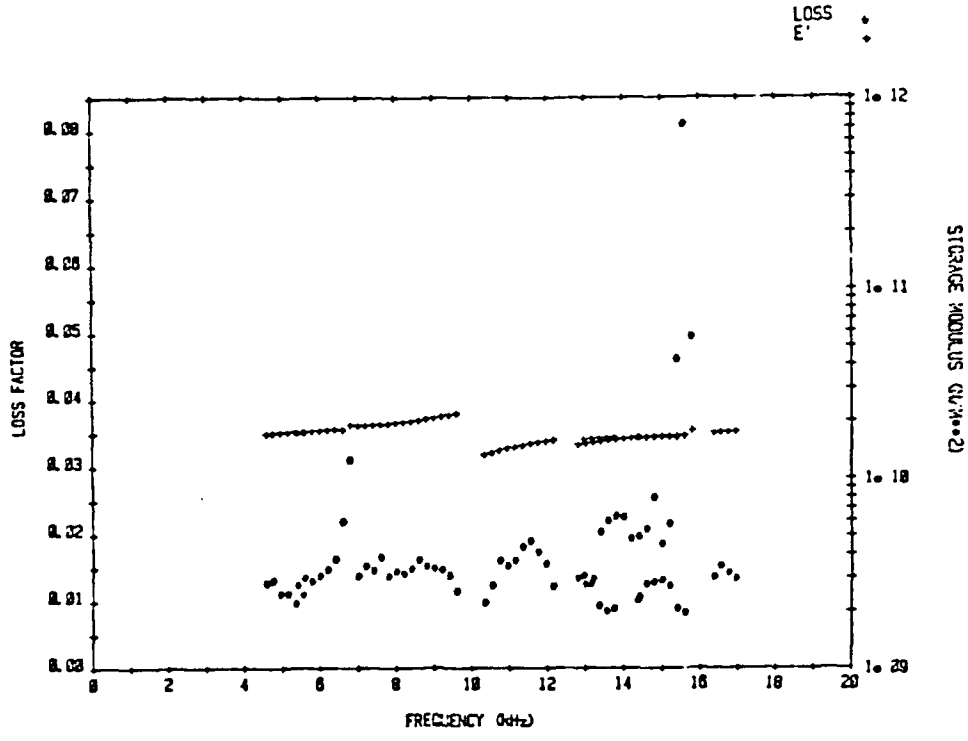

Figure 4.6 - Loss Factor and Storage Modulus Versus Frequency for a Polyethylene/60% PZT Sample.

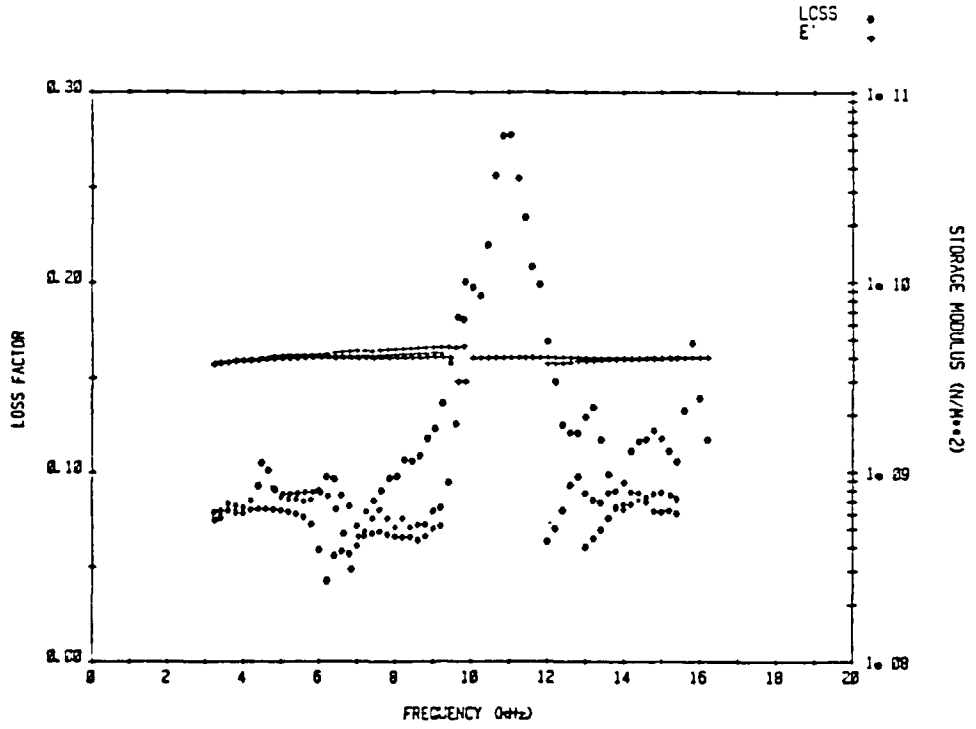

Figure 47a - Loss Factor and Storage Modulus Versus Frequency for a Polypropylene Sample.

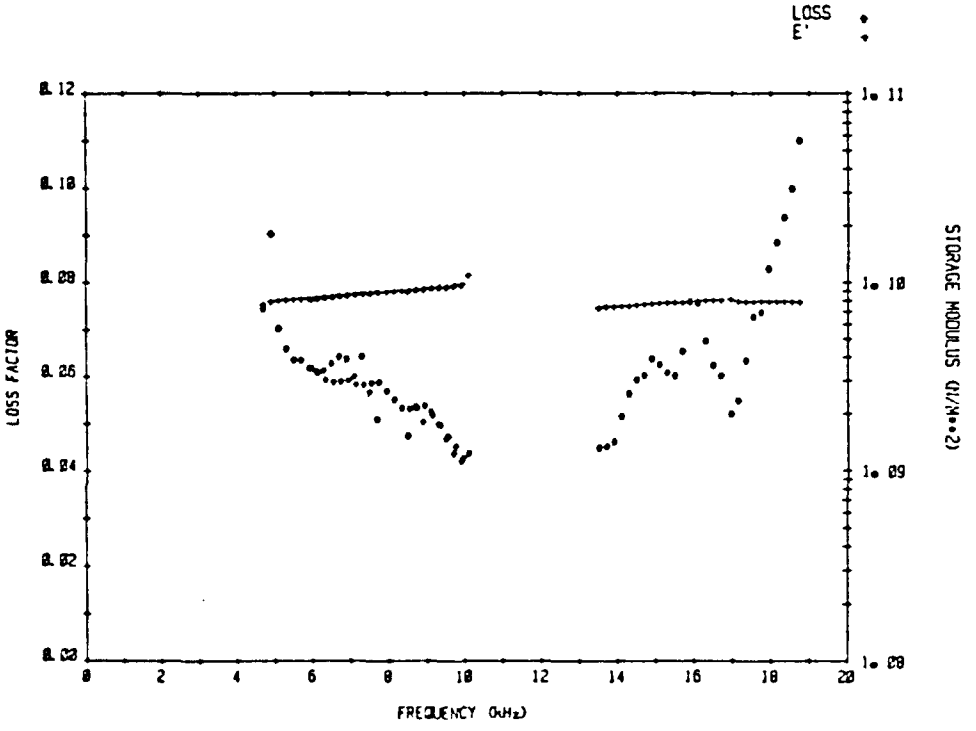

Figure 47b - Loss Factor and Storage Modulus Versus Frequency for a Polypropylene/25% TiO_2 Sample.

there is a readily discernable loss factor peak. Figure 4.7a shows that the loss factor and storage modulus for three tests using three different end masses agree fairly well with each other.

A 25% anatase and polypropylene composite was used for the tests whose results are shown in Fig. 4.7b. The anatase must also act to stiffen the composite because the loss factor decreases and the storage modulus increases over the values for polypropylene alone. The loss factor initially decreases and then shows a sharp increase at the higher frequencies. It is possible that the loss factor peak occurs near 18 or 19 kHz. Another possibility is that the transition frequency (between the "rubbery" and "glassy" regions) occurs at a much lower frequency, say around 2 kHz. However, this would not explain the sharp peak near 18 kHz.

4.5 Polychloroprene Composites

Two samples containing polychloroprene were tested. One consisted of only polychloroprene and the other contained 25% PZT by volume. Comparing Figs. 4.8a (no PZT) and 4.8b, it can be seen that the decrease in damping due to the addition of PZT is compensated by the interaction between the polychloroprene matrix and the PZT particles. The PZT particles must resonate with the matrix material causing additional friction losses. Notice that the storage modulus still increases with the addition of PZT particles by nearly a factor of three. Fig. 4.8a shows a distinct peak in the loss factor near 6 kHz. The loss factor curve in Fig. 4.8b appears to follow

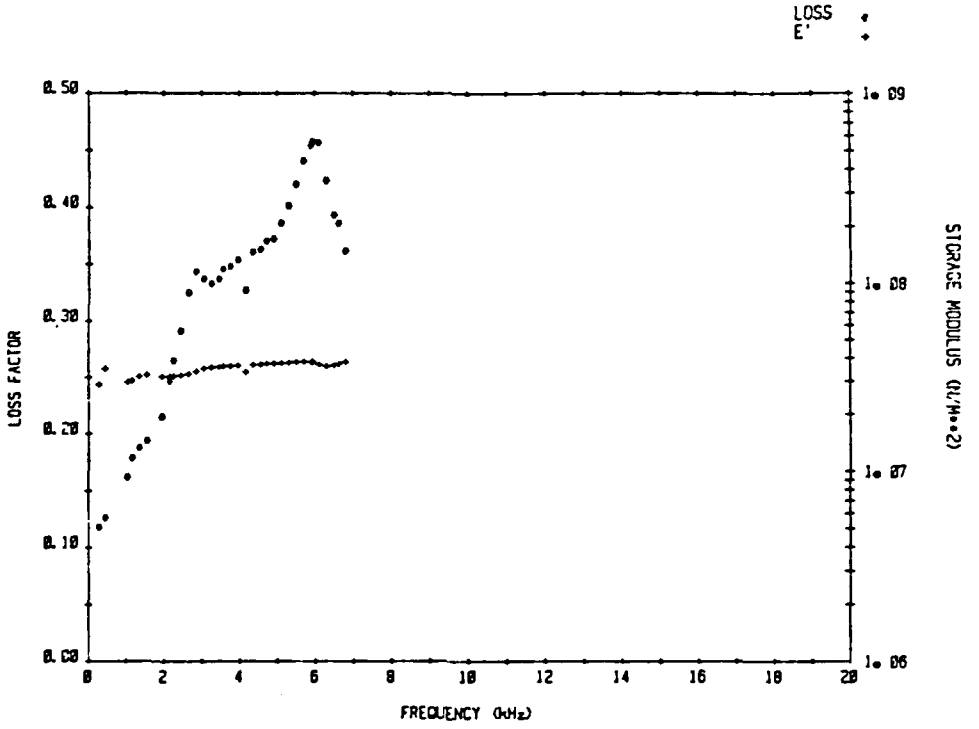

Figure 4.8a - Loss Factor and Storage Modulus Versus Frequency for a Polychloroprene Sample.

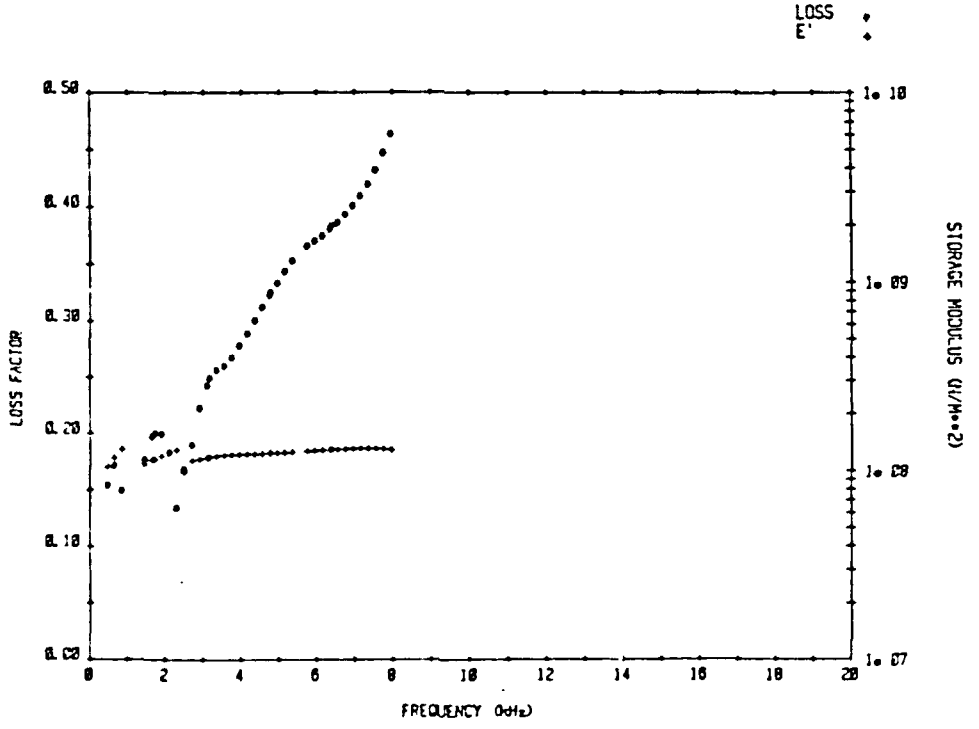

Figure 4.8b - Loss Factor and Storage Modulus Versus Frequency for a Polychloroprene/25% PZT Sample.

the same pattern except that it is shifted higher in frequency by about 2 kHz. This lends credence to the idea that increasing the percentage of PZT, or any dense filler, will shift the loss factor curve of the polymer composite to a higher frequency.

4.6 Spurrs Epoxy Composites

Spurrs epoxy is another low-damping material. The loss factor, as shown in Fig. 4.9, ranges between 0.03 and 0.045 for the two separate tests conducted. The two sets of test results show a discrepancy in the loss factor at frequencies between 9 and 12 kHz. This could be a result of variations in the cure time of the epoxy used to bond the specimen to the test fixtures or it might be related to the difference in the end mass used. For low damping materials the effect of insufficent cure time will be magnified. The cure time was kept fairly constant so this large a discrepany is probably a result of the larger end mass causing an increase in the stress amplitude through the sample. This occurs with metals subjected to cyclical stress when the fatigue limit is approached [7]. It is not known if the stress amplitude is great enough to cause plastic slip or flow in the polymeric samples.

The same problem of loss factor discrepancies also occurs with the results shown in Figs. 4.10a and 4.10b. Both composites used for these tests are composed of 25% PZT and Spurrs epoxy. For the higher frequencies, the storage moduli compare well, but the loss factors do not.

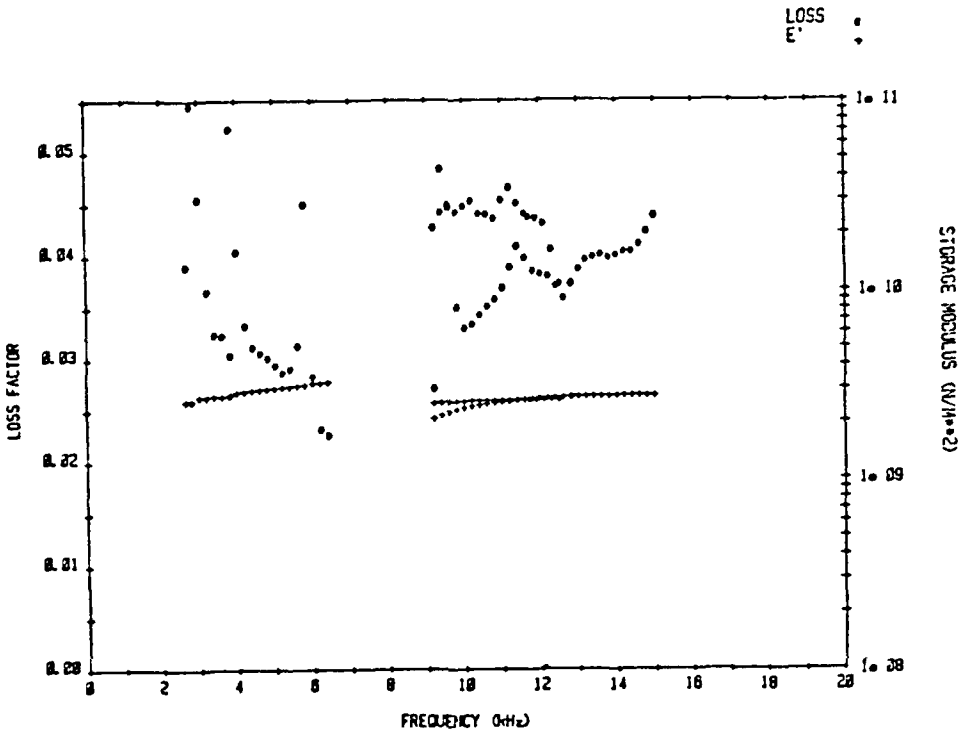

Figure 4.9 - Loss Factor and Storage Modulus Versus Frequency for a Spurrs Epoxy Sample.

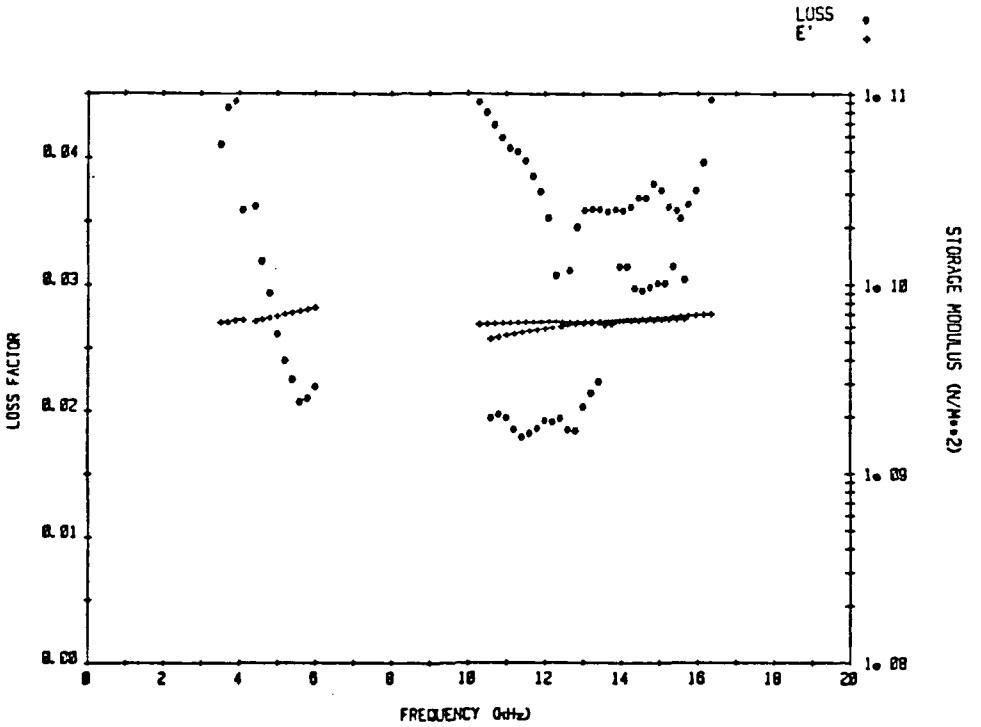

Figure 4.10a - Loss Factor and Storage Modulus Versus Frequency for a Spurrs Epoxy/25% PZT Sample (No.1).

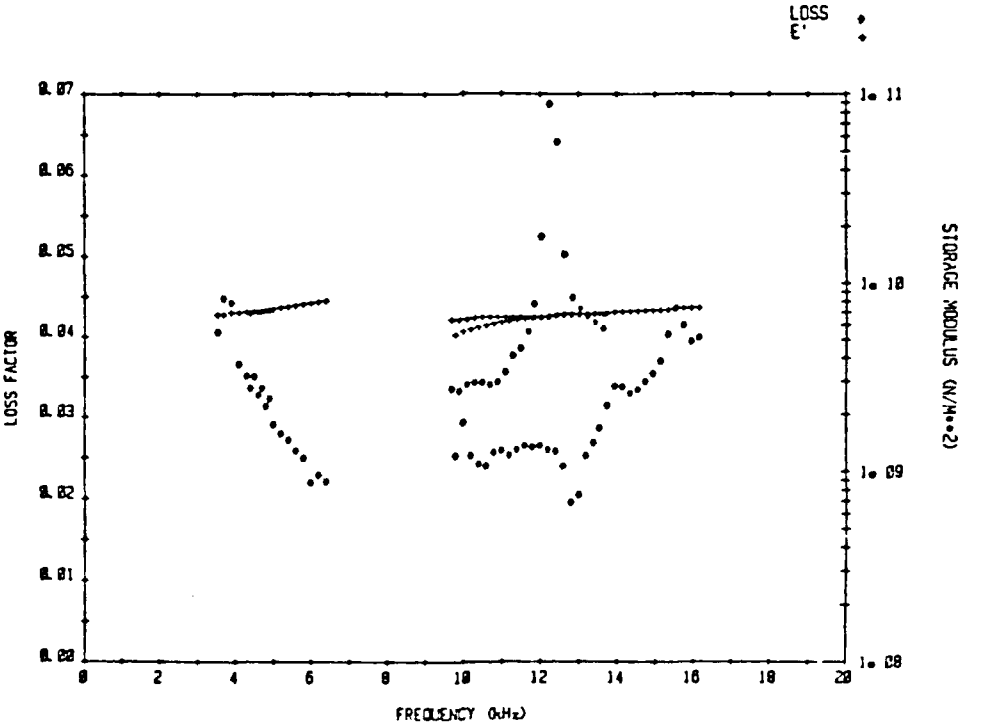

Figure 4.10b - Loss Factor and Storage Modulus Versus Frequency for a Spurrs Epoxy/25% PZT Sample (No. 2).

Again, the higher-valued loss factor curve corresponds to the test using the larger end mass. The upper loss factor curve in Fig. 4.10b (two tests are shown in this figure) contains a sharp peak near 12 kHz. It looks like the upper loss factor curve shown in Fig. 4.10a might have a peak near 10 kHz. However, neither of the two lower curves shows a peak.

For granular materials the loss factor increases markedly with increasing stress amplitude, especially if the acceleration approaches the acceleration of gravity [6]. Unfortunately, the definition of "granular" is somewhat vague. If the PZT-polymer composites could be considered granular, then tests run with larger end masses should show higher damping levels. This indeed was the case with the results shown in Figs. 4.10a and 4.10b.

4.7 Test Results for Additional Materials

The four additional polymeric materials tested provided good results. The test conducted using aluminum yielded only a few valid points. The measured storage modulus compares well with values typically quoted for the Young's Modulus of aluminum (7.0×10^{10} N/m^2). The measured loss factor for the first mode was 0.002 which is much larger than the damping of most aluminum alloys ($\eta_{alum} = 0.0001$) [6]. This indicates that the inherent damping of the test system dominates the results for very low values of damping. The system losses consist of epoxy losses, brass fixture losses, and the losses caused by the effect of the accelerometer cables. These

sources of additional damping effectively limit the present test setup to materials with a loss factor no smaller than 0.002.

Figure 4.11a is a plot of the storage modulus and loss factor for SOAB. SOAB is an acronym for a SOund ABsorbing material marketed by B. F. Goodrich Co.. It consists of aluminum particles embedded in butyl. SOAB had the largest loss factor of any material tested; it had a peak loss factor near 1.3. The η and E' curves for SOAB are reasonably smooth and continuous.

A sample of the Nippon Electric Company (NEC) composite discussed in Chapter 1 was tested. The loss factor and storage modulus plots are shown in Fig. 4.11b. Approximate values for the loss factor and storage modulus of this type of composite [27] are η=0.35 and E'= 1.8 x 10^9 N/m^2. The present test results give slightly higher damping values and slightly lower storage modulus values.

The plot of the dynamic properties for the neoprene specimen resembles the plots of the Eccogel composites. The loss factor, shown in Fig. 4.12a, peaks near 3 kHz with a value of 0.78. This result is quite believable. The storage modulus is low (1.0 x 10^7 N/m^2) like that of the Eccogel composites.

The final plot, Fig. 4.12b, shows the dynamic properties of a polyurethane sample. The loss factor curve generally increases with increasing frequency. The regions where the loss factor tends to decrease correspond to frequencies near the 0° phase points of the transfer ratio, where valid data could not be obtained. Both the loss factor and storage

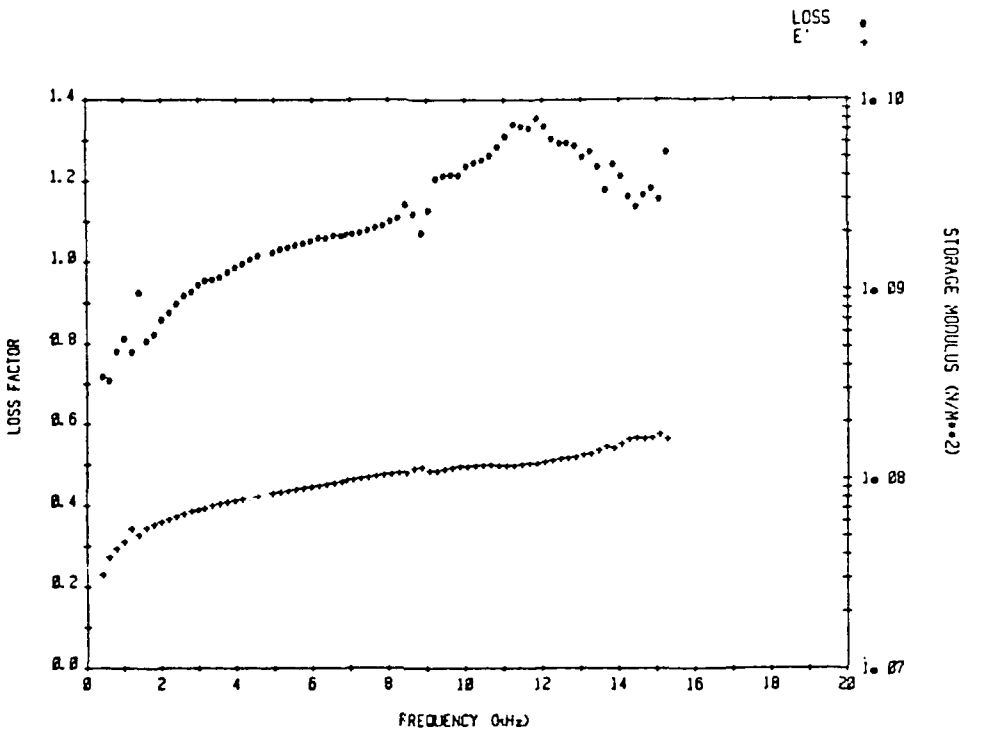

Figure 4.11a - Loss Factor and Storage Modulus Versus Frequency for a SOAB Sample.

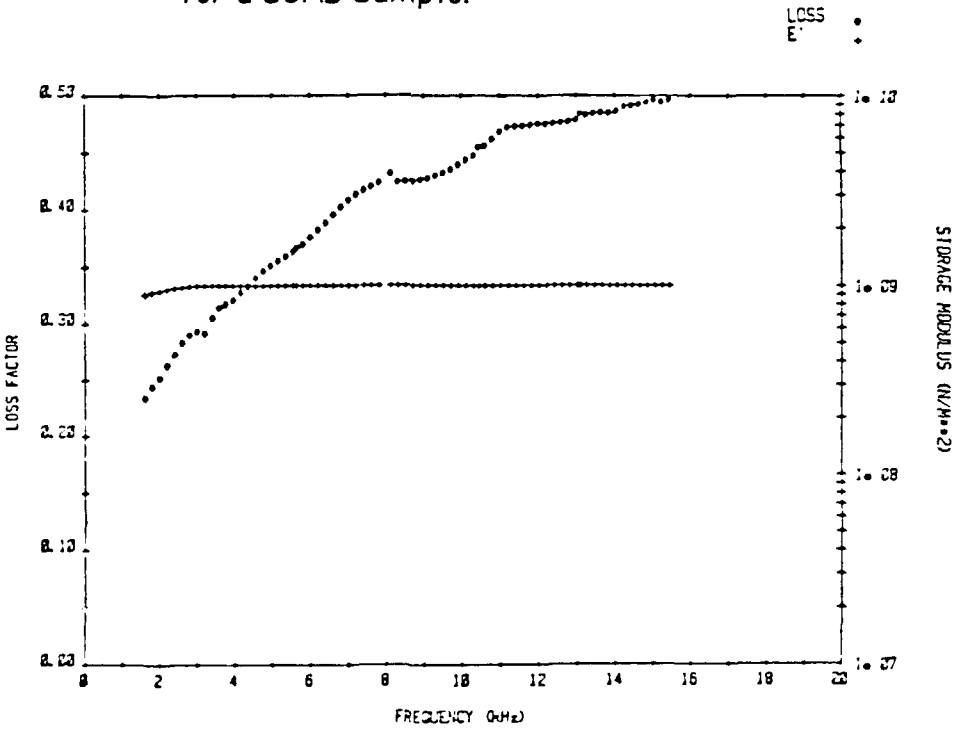

Figure 4.11b - Loss Factor and Storage Modulus Versus Frequency for a NEC Composite Sample.

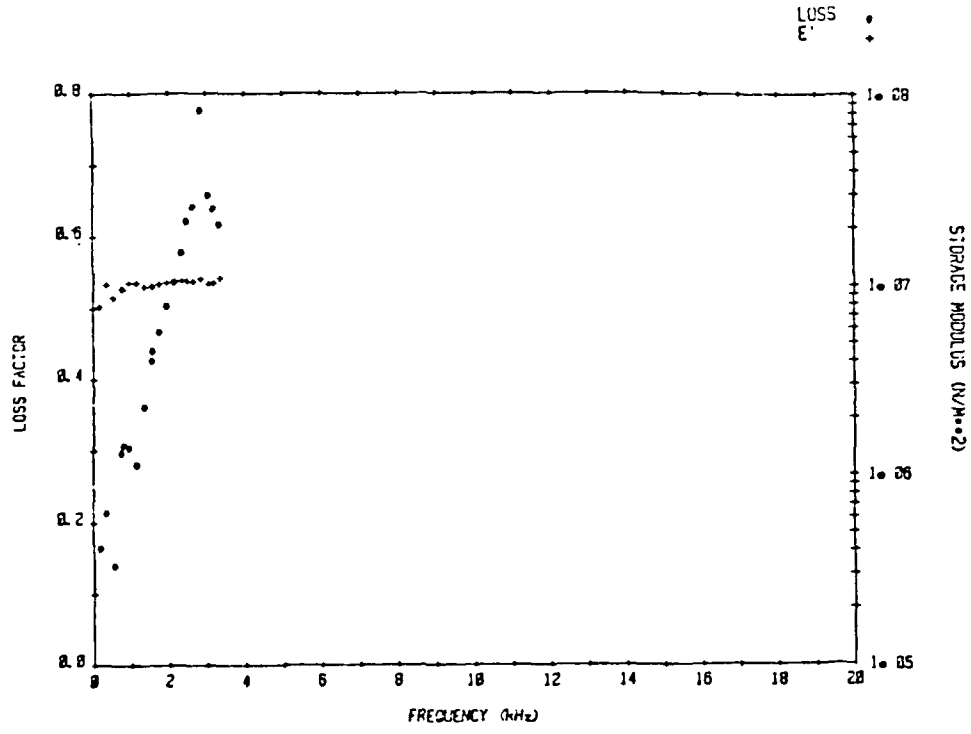

Figure 4.12a - Loss Factor and Storage Modulus Versus Frequency for a Neoprene Sample.

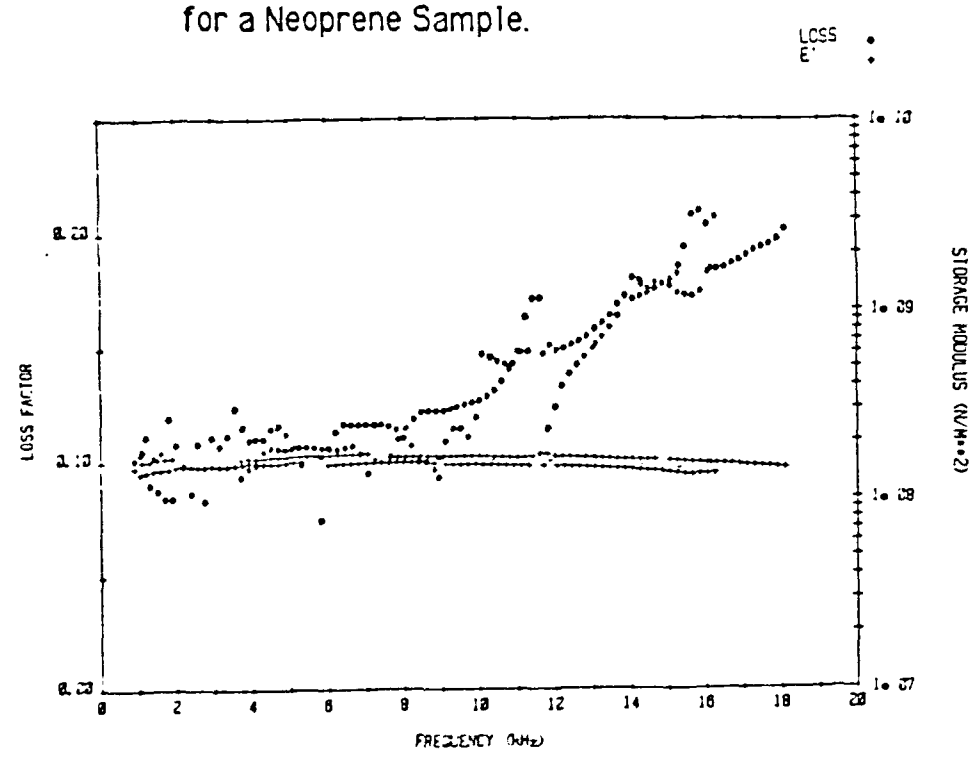

Figure 4.12b - Loss Factor and Storage Modulus Versus Frequency for a Polyurethane Sample.

4.8 Comparison of the Test Results

The loss factor and storage modulus test results for the various test materials are compared to each other and to some storage modulus values obtained using an ultrasonic pulse-echo technique at about 3.0 MHz [26] in Table 4.1. The materials are listed in order of decreasing loss factor. The high-damping materials ($\eta \geq 0.1$) are compared at 2 kHz and the lower-damping materials are compared at 5 kHz. The ultrasonic frequency storage modulus values should be a little larger than the storage modulus values obtained in the acoustic range because the storage modulus slopes slightly upward in the "glassy" region. This is indeed the case for materials tested using both methods.

Additional comparisons with published results are shown in Table 4.2. It is virtually impossible to compare results of identical materials since one blend of a polymer will inevitably differ in composition from another. Variations in aging, temperature, or frequency can also change material properties considerably. The purpose of the comparisons is simply to provide another check against gross errors in the results.

Table 4.1 Comparison of Loss Factor and Storage Modulus Results at Common Frequencies.

Material	Frequency	Loss Factor	Storage Modulus	
			Acoustic	Ultrasonic* Pulse/Echo
	kHz		N/m^2	N/m^2
Eccogel	2.0	0.87	3.78×10^6	
SOAB	2.0	0.86	5.89×10^7	
Eccogel/10% PZT	2.0	0.80	7.27×10^6	
Eccogel/25% PZT	2.0	0.67	3.27×10^7	
Neoprene	2.0	0.51	1.03×10^7	
NEC Composite	2.0	0.25	9.39×10^8	
Polychloroprene	2.0	0.22	3.19×10^7	
Polychloroprene/25% PZT	2.0	0.19	1.22×10^8	
Polyurethane	2.0	0.11	1.42×10^8	
Polypropylene	5.0	0.080	3.96×10^9	
Polypropylene/25% TiO_2	5.0	0.063	7.80×10^9	
Polyethylene	5.0	0.035	3.07×10^9	5.63×10^9
Spurrs Epoxy	5.0	0.029	3.05×10^9	5.46×10^9
Spurrs Epoxy/25% PZT	5.0	0.028	6.99×10^9	
Polyethylene/25%PZT	5.0	0.015	6.94×10^9	8.25×10^9
Polyethylene/60%PZT	5.0	0.011	1.75×10^{10}	2.28×10^{10}

* - at 3 MHz

Table 4.2 Comparison of Loss Factor and Storage Modulus Values with Those of Other Studies.

Material	Frequency	This Study		Other Study		Reference
		η	E'	η	E'	
	(kHz)		(N/m^2)		(N/m^2)	
NEC Composite	—	0.41	1.0×10^9	0.35	1.8×10^9	[1]
Polyurethane	2.0	0.11	1.4×10^8	0.15	1.2×10^8	[4]
Polypropylene	—	0.08	4.0×10^9	0.11	2.6×10^9	[29]
Aluminum	—	0.002	7.0×10^{10}	0.0001	7.0×10^{10}	[6]

CHAPTER 5

CONCLUSIONS AND SUMMARY

5.1 Conclusions

The loss factor and storage modulus results quoted here compare closely with those of other researchers for similar materials. The results for high-damping materials are more characteristic of viscoelastic materials than are the results for low-damping materials. This is probably a consequence of the PZT material being an elastic material since most of the unusual results occur with the addition of PZT. A good example is the difference between Eccogel with 25% PZT, Eccogel with 10% PZT, and pure Eccogel. While pure Eccogel and Eccogel with 10% PZT have a discernable loss factor peak, this peak disappears when the percentage of PZT is increased to 25%.

In every case except one, adding PZT to a polymer had the effect of decreasing the loss factor. Only with polychloroprene did the damping not decrease appreciably with the addition of PZT. This probably is a result of the PZT mass particles resonating with the compliance of the polymer. Although Eccogel is also a very high-damping polymer, it is not as dense as polychloroprene and thus it may not provide enough frictional resistance to the vibrating PZT particles. This effect is most likely responsible for the high damping in the NEC composite where ferrite particles resonate with

the polyester resin matrix.

The test of an aluminum sample effectively set the lower limit for damping measurements. Any material with a loss factor less than 0.002 can not be tested accurately by the measuring system used here because the inherent system losses will obscure the material damping. Since the primary application of the Transfer Function Method is to test viscoelastic or rubbery specimens this lower limit should not pose a problem. If very low damping materials are to be tested, either the sytem losses must be decreased or another dynamic modulus test procedure must be used.

One disadvantage of the Transfer Function Method is that results can not be obtained for frequencies lower the first bar resonance. For some of the low damping composites this first resonance was as high as 3 kHz. If loss factor values could be obtained for the very low frequencies then many of the transition peaks could be discerned. The Spurrs epoxy samples appear to have transition frequencies lower than the first resonance. The supporting evidence for this is the decreasing loss factor values at low frequencies shown in Figs. 4.9, 4.10a, and 4.10b. The loss factor peak for these samples probably occurs before the first resonance.

Most of the composites containing 25% or more PZT are characterized by relatively flat storage modulus curves. Typical loss factor and storage modulus values for this type of PZT are $\eta = 0.002$, and $E' = 8 \times 10^{10}$ N/m^2 [28]. The PZT may act to stiffen the composite so that the elastic modulus resembles that of a ceramic more than that of a viscoelastic material.

Some of the polymers also show very gradually increasing storage moduli (e.g., Fig. 4.9). The probable cause for this behavior is that the polymer has already entered the "glassy" region. The loss factor peak probably occurred at a frequency below the primary resonance.

5.2 Summary

For applications at room temperature and in the audible frequency range, the Transfer Function Method appears to be a reasonable method for measuring the storage modulus and loss factor of a viscoelastic material. The primary difficulty in using it is that the solutions to Eqs. (2.2) and (2.3) become suspect after the first few modes if the starting iteration seed is not close to the correct solution. Equations (2.2) and (2.3) may look imposing but with the aid of the three-dimensional plots the behavior can be readily understood. From this point it was a simple matter to develop an algorithm guaranteeing convergence to the correct solution. The algorithm developed during this study to seed the equations to the correct values is simple, yet works well.

The other improvement made to the Transfer Function Method was to account for the effect of lateral vibrations in the bar. This correction can easily change both the loss factor and storage modulus by 10% or more at the higher frequencies. It should not be neglected as commonly practiced when using the Transfer Function Method.

Although the loss factor and storage modulus plots may still be subject

to some experimental error, they are useful from the standpoint that a comparison of the damping between different polymer composites can be made with confidence. The test results also seem to indicate that the method is capable of providing reproducible results. These two requirements were considered the most important to meet when the decision to develop a test procedure for measuring the damping properties of the PZT-polymer composites was made.

The primary attributes of the Transfer Function Method, with the improvements made during this study, are that it is very fast, easy to perform, can be implemented at modest cost, is capable of testing viscoelastic materials in a wide range of sizes, and requires almost no operator judgment.

5.3 Recommendations for Further Study

The test setup in its present form is useful but with the proper modifications it could become much more versatile and accurate. The first improvement that could be undertaken would be to decrease the inherent system damping. This could be accomplished by using noncontact transducers for determining the acceleration ratio of the mass-loaded and driven ends. If the system losses could be reduced to the losses associated with air friction then this test arrangement could be used to test very low damping materials such as metals.

Another improvement would be to solve Eqs. (2.2) and (2.3) for the loss factor and storage modulus at frequencies below the primary resonance. The same extrapolation procedure used to approximate seed values beyond the last mode could also be used to seed the Newton-Raphson iteration procedure for frequencies smaller than the first mode resonance frequency provided the amplitude and phase data were accurate. This would provide valuable low frequency data. The behavior of the dynamic modulus at low frequencies seems to be important because it appears that for many composites the transition frequency is below 2 kHz.

One final improvement to the method would be to extend the testing procedure to include torsional vibrations. The equations of motion are the same as for the longitudinal vibrations except that the material and displacement parameters change. If both the complex elastic and shear moduli could be determined, the complex Poisson's ratio could also be found by using relationships among the various elastic constants. This would probably necessitate that physical changes be made to the testing apparatus. However, the software changes would probably be minimal.

APPENDIX A

Derivation of equations used to solve for loss factor and storage modulus.

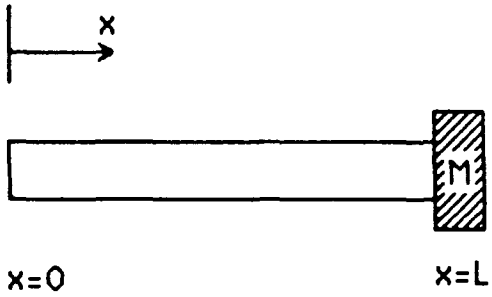

A= cross-sectional area of the bar.
M= the end mass.
E*= complex elastic modulus.
k= complex propagation constant.
F= force on the cross-section.

Assume a solution of the one dimensional, reduced, wave equation of the form:

$u(x)= C_1 \cos kx + C_2 \sin kx$ $\quad$ u(x)= longitudinal displacement of the bar.

$u(0)= U_0$ $\quad$ U_0= displacement at x=0 and t=0.

The axial force in the bar at any position x is given by:

$$F= -AE^* \partial u/\partial x \tag{A.1}$$

The boundary conditions are:

@ x=0 $\quad$ $u(0,t)= C_1= U_0$ (A.2)

@ x=L $\quad$ $F= M \partial^2 u/\partial t^2= -M\omega^2 u(L)$ (A.3)

Therefore:

$$-AE^* \partial u/\partial x\Big|_{x=L} = -M\omega^2 u(L) \tag{A.4}$$

Applying the solution for u(x) yields:

$$AE^*k[-U_0 \sin kL + C_2 \cos kL]= M\omega^2[U_0 \cos kL + C_2 \sin kL] \tag{A.5}$$

or

$$C_2[M\omega^2 \sin kL - AE^*k \cos kL] = -[AE^*kU_0 \sin kL + M\omega^2 U_0 \cos kL] \tag{A.6}$$

thus,

$$C_2 = \frac{U_0[\, AE^*k \sin kL + M\omega^2 \cos kL]}{AE^*k \cos kL - M\omega^2 \sin kL} \tag{A.7}$$

$$= \frac{U_0[\, \tan kL + \gamma]}{[1 - \gamma \tan kL]} \qquad \text{where} \quad \gamma = \frac{M\omega^2}{AE^*k} \tag{A.8}$$

The ratio of displacement of driven end to that of the mass loaded end is therefore:

$$\frac{u(0)}{u(L)} = \frac{U_0}{u(L)} = \frac{U_0}{U_0 \cos kL + \dfrac{U_0[\, \tan kL + \gamma]}{[1 - \gamma \tan kL]} \sin kL} \tag{A.9}$$

$$= \frac{1 - \gamma \tan kL}{[(\cos kL - \gamma \sin kL) + (\tan kL \sin kL + \gamma \sin kL)]} \tag{A.10}$$

$$= \cos kL - \gamma \sin kL \tag{A.11}$$

The complex wave propagation constant can be written

$$k = (\rho\omega^2/E^*)^{-1/2} \tag{A.12}$$

$$kL = \omega L(\, \rho/E' e^{i\delta})^{-1/2} = \frac{\omega L\, e^{i\delta/2}}{(E'/\rho)^{1/2}} \tag{A.13}$$

$$= \frac{\omega L}{(E'/\rho)^{1/2}} [\cos(\tfrac{\delta}{2}) - i \sin(\tfrac{\delta}{2})] \tag{A.14}$$

$$= \frac{\omega L}{(E'/\rho)^{1/2} \sec(\frac{\delta}{2})} [1 - i \tan(\tfrac{\delta}{2})] \tag{A.15}$$

but,

$$c = \text{the phase velocity} = (E'/\rho)^{1/2} \sec(\tfrac{\delta}{2}) \tag{A.16}$$

$$\xi = \omega L/c \tag{A.17}$$

Thus,

$$kL = \xi[1 - i \tan(\tfrac{\delta}{2})] = \xi\,(1 - i\Omega) \tag{A.18}$$

$$\text{where } \Omega = \tan(\tfrac{\delta}{2}) \tag{A.19}$$

$$\gamma = \frac{M\omega^2}{AE^*k} = \frac{M\omega^2}{A(\rho\omega^2/k^2)k} = \frac{MkL}{A\rho L} = RkL \qquad (A.20)$$

$$= R\xi[1-i\Omega] \qquad \text{where R is the mass ratio} \qquad (A.21)$$

$$= M/\rho AL$$

Plugging in γ and k into (A.11) yields:

$$\cos kL - \gamma \sin kL = \cos\xi(1-i\Omega) - R\xi(1-i\Omega)\sin\xi(1-i\Omega) \qquad (A.22)$$

Expansions for the complex sine and cosine are:

$$\cos(x-iy) = \cos x \cosh y + i\sin x \sinh y \qquad (A.23)$$

$$\sin(x-iy) = \sin x \cosh y - i\cos x \sinh y \qquad (A.24)$$

Using the above identities and Eq. (A.11)

$$\frac{u(0)}{u(L)} = \frac{U_0}{u(L)} = \cos kL - \gamma \sin kL$$

$$= \cos\xi\cosh\xi\Omega + i\sin\xi\sinh\xi\Omega - R\xi(1-i\Omega)[\sin\xi\cosh\xi\Omega - i\cos\xi\sinh\xi\Omega] \qquad (A.25)$$

This can be expressed in terms of a real part, T_R, and an imaginary part, T_I, as:

$$T_R = \cosh\xi\Omega[\cos\xi - R\xi\sin\xi] + R\xi\Omega\cos\xi\sinh\xi\Omega \qquad (A.26)$$

and

$$T_I = \sinh\xi\Omega[\sin\xi + R\xi\cos\xi] + R\xi\Omega\sin\xi\cosh\xi\Omega \qquad (A.27)$$

BIBLIOGRAPHY

1. "New Ferrite Compound Reduces Vibration and Noise," Business Japan , 143, (May, 1982).

2. W. M. Madigosky and G. F. Lee, "Improved Resonance Technique for Materials Characterization," J. Acoust. Soc. Am. , 73 (4), pp. 1374-1377, (1983).

3. T. Pritz, "Tranfer Function Method for Investigating the Complex Modulus of Acoustic Materials: Rod-Like Specimen," J. Sound and Vibration , 81 (3), pp. 359-376, (1982).

4. R. N. Capps, "Dynamic Young's Moduli of Some Commercially Available Polyurethanes," J. Acoust. Soc. Am. , 73 (6), pp. 2000-2005, June 1983.

5. D. M. Norris Jr. and W. C. Young, "Complex Modulus Measurement by Longitudinal Vibration Testing," Exp. Mech. , 10, pp. 93-96, (1970).

6. E. E. Ungar, "Damping of Panels," in Noise and Vibration Control , ed. L. L. Beranek, chap 14, p. 434, (1971).

7. B. J. Lazan and L. E. Goodman, "Material and Interface Damping," in Shock and Vibration Handbook , eds. C. M. Harris and C. E. Crede, vol 2., 36-1, (1961).

8. B. J. Lazan, "Energy Dissipation Mechanisms in Structures, with Particular Reference to Material Damping," Structural Damping , ed. J. E. Ruzicka, ASME, 1-34, (1959).

9. J. C. Snowdon, Vibration and Shock in Damped Mechanical Systems , New York: John Wiley and Sons Inc., 3, (1968).

10. Brüel & Kjær Technical Review No. 1 (1958), "Measurement of the Complex Modulus of Elasticity."

11. Brüel & Kjær Application Notes, "Measurement of the Complex Modulus of Elasticity: A Brief Survey."

12. N. S. Timmerman, "Assessment of Dynamic Modulus Testing Facilities," Bolt Beranek and Newman Inc. Technical Memorandum No. 652, March 1982.

13. S. L. Quimby, "On the Experimental Determination of the Viscosity of Vibrating Solids," Phys. Rev. , 25, pp. 558-573, (1925).

14. R. K. Galkiewicz and F. E. Karasz, "Viscoelastic Characterization of Isotropic Solids Using Harmonic Dispersion of Longitudinal Resonances," J. Appl. Phys. , 49 (10), pp. 5233-5240, October 1978.

15. B. G. Ferguson, "Calculation of The Loss Tangent for Viscoelastic Materials Using the Triple-Bar Composite Resonance Technique," J. Acoust. Soc. Am. , 76 (5), pp. 1577-1579, (1984).

16. C. M. Cannon, A. D. Nashif and D. I. G. Jones, "Damping Measurements on Soft Viscoelastic Materials Using a Tuned Damper Technique," 1968 Shock and Vibration Bulletin , 38, pp. 151-163, (1968).

17. D. I. G. Jones and M. L. Parin, "Technique for Measuring Damping Properties of Thin Viscoelastic Layers," J. Sound and Vibration , 24 (2), pp. 201-210, (1972).

18. T. M. Lee, "Method of Determining Dynamic Properties of Viscoelastic Solids Employing Forced Vibration," J. Appl. Phys. , 34, pp. 1524-1529, (1963).

19. W. M. Madigosky and G. F. Lee, "Automated Dynamic Young's Modulus and Loss Factor Measurements," J. Acoust. Soc. Am., 66 (2), pp. 345-349, (1979).

20. T. E. Shoup, A Practical Guide to Computer Methods for Engineers, Prentice Hall, Englewood Cliffs, N. J., pp. 33-36, (1979).

21. J. D. Ferry, Viscoelastic Properties of Polymers, 2nd Ed., Wiley, New York, (1970).

22. C. Chree, "The Equations of an Isotropic Elastic Solid in Polar and Cylindrical Coordinates, Their Solutions and Applications," Trans. Cambridge Phil. Soc., 14, pp. 250-369, (1889).

23. G. A. Coquin, "Attenuation of Guided Waves in Isotropic Viscoelastic Materials," J. Acoust. Soc. Am., 36 (6), pp. 1074-1080, (1964).

24. T. Pritz, "Apparent Complex Modulus of a Longitudinally Vibrating Viscoelastic Rod," J. Sound and Vibration, 77 (1), pp. 93-100, (1981).

25. A. E. H. Love, A Treatise on the Mathematical Theory of Elasticity, 4th ed., Dover, New York, (1944).

26. S. Pilgrim, Personal Communication, June 27, 1985.

27. F. Yamauchi and S. Emoto, "Ferrite-Resin Composite Material for Vibration Damping," Resources and Environment Research Labs., NEC Corporation, 1-1, Miyazaki, Kawasaki-City, Kanagawa 213, Japan.

28. Catalog Number 761-101, Channel Industries, Inc., 839 Ward Dr., Santa Barbara, CA 93111.

29. D. V. Wright and R. L. Bannister, "Plastic Models for Structural Analysis," Scientific Paper 69-1E7-TAEUG-P1, Westinghouse Electric Corporation, July 1969.

UNCLASSIFIED DISTRIBUTION LIST FOR ARL TM No. 85-138, "Improvements to the Transfer Function Method for Determining the Complex Dynamic Modulus of Polymer Composites," by A. E. Semple and W. Thompson, Jr., dtd 5 August 1985.

Office in Charge
Naval Surface Weapons Center
Detachment
White Oak Laboratory
Silver Spring, MD 20910

Attn: Dr. Walter M. Madigosky
(Copy No. 1)

Director
Naval Research Lab.
Underwater Sound Reference
Detachment
P. O. Box 8337
Orlando, FL 32856

Attn: Dr. Rodger N. Capps
(Copy No. 2)

The Pennsylvania State University
Dept. of Eng. Science & Mechs.
133 Hammond Bldg.
University Park, PA 16802

Attn: Prof. Vernon Neubert
(Copy No. 3)

The Pennsylvania State University
Dept. of Polymer Science
313 Steidle Bldg.
University Park, PA 16802

Attn: Prof. James P. Runt
(Copy No. 4)

The Pennsylvaina State University
140 Materials Res. Lab.
University Park, PA

Attn: Library
(Copy No. 5)

Commander
Naval Underwater Systems Center
Department of the Navy
Newport, RI 02840

Attn: Library
(Copy No. 6)

Commander
Naval Ocean Systems Center
Department of the Navy
San Diego, CA 92152

Attn: Library
(Copy No. 7)

Commander
Office of Naval Research
Department of the Navy
800 N. Quincy St.
Arlington, VA 22217-5000

Attn: Dr. Robert Pohanka
(Copies No. 8 and 9)

Commander
Naval Sea Systems Command
Deparmtment of the Navy
Washington, DC 20362

Attn: Code SEA 9961 (Library)
(Copies No. 10 and 11)